Int J Earth Sci (Geol Rundsch) (2007) 96:817–841
DOI 10.1007/s00531-006-0141-3

ORIGINAL PAPER

Archaean high-K granitoids produced by remelting of earlier Tonalite–Trondhjemite–Granodiorite (TTG) in the Sangmelima region of the Ntem complex of the Congo craton, southern Cameroon

Cosmas Kongnyuy Shang · Muharrem Satir · Emmanuel Nkonguin Nsifa · Jean-Paul Liégeois · Wolfgang Siebel · Heiner Taubald

Received: 4 August 2005 / Accepted: 19 October 2006 / Published online: 8 December 2006

Abstract We present a geochemical and isotopic study that, consistent with observed field relations, suggest Sangmelima late Archaean high-K granite was derived by partial melting of older Archaean TTG. The TTG formations are sodic-trondhjemitic, showing calcic and calc-alkalic trends and are metaluminous to peraluminous. High-K granites in contrast show a potassic calc-alkaline affinity that spans the calcic, calc-alkalic, alkali-calcic and alkalic compositions. The two rock groups (TTG and high-K granites) on the other hand are both ferroan and magnesian. They have a similar degree of fractionation for LREE but a different one for HREE. Nd model ages and Sr/Y ratios define Mesoarchaean and slab-mantle derived magma compositions respectively, with Nb and Ti anomalies indicating a subduction setting for the TTG. Major and trace element in addition to Sr and Nd isotopic compositions support field observations that indicate the derivation of the high-K granitic group from the partial melting of the older TTG equivalent at depth. Geochemical characteristics of the high-K granitic group are therefore inherited features from the TTG protolith and cannot be used for determining their tectonic setting. The heat budget required for TTG partial melting is ascribed to the upwelling of the mantle marked by a doleritic event of identical age as the generated high-K granite melts. The cause of this upwelling is related to linear delamination along mega-shear zones in an intracontinental setting.

Keywords High-K granites · TTG · Partial melting · Major and trace element composition · Sr and Nd systematics

C. K. Shang (✉) · M. Satir · W. Siebel · H. Taubald
Institute of Geosciences, University of Tuebingen,
Wilhelmstrasse 56, 72074 Tuebingen, Germany
e-mail: shang004@yahoo.com; cosmas@uni-tuebingen.de

E. N. Nsifa
Department of Earth Sciences,
University of Yaounde I,
BP 812, Yaounde, Cameroon
e-mail: nnsifa@yahoo.fr

J.-P. Liégeois
Isotope Geology Section, Africa Museum,
B-3080 Tervuren, Belgium
e-mail: jean-paul.liegeois@africamuseum.be

Introduction

Archaean cratons are mostly composed of magmatic rocks of the Tonalite–Trondhjemite–Granodiorite (TTG e.g. Jahn et al. 1981; Martin et al. 1983) suite and greenstone belt rock formations that are an association of metasediments and mafic-ultramafic intrusive rocks. The study of these rock formations has led to proposals about early crustal growth (e.g. Glikson 1979; Shirey and Hanson 1986; Luais and Hawkesworth 1994; Moorbath and Kamber 1998; Windley 1998; Foley et al. 2002; Lobach-Zhuchenko et al. 2003; Sharma and Pankit 2003). Granites and particularly high-K granites are generally younger than TTG and greenstone belts and are often thought to constitute the last major magmatic phase in Archaean terranes. Late K-rich granites in the Ntem complex of the Congo craton (Shang et al. in preparation and this study), occur as intrusions clearly distinct from the older TTG (Shang et al. 2004a, b). Various workers (e.g. Stern and

Hanson 1991; Evans and Hanson 1992; Tepper et al. 1993; Jayananda et al. 1994; Wickham 1987; Wickham et al. 1995; Rapp 1997) have described different models of granitoid genesis but two main ones can account for the genesis of granites: (1) direct fractional crystallization of a mantle mafic magma, with or without crustal assimilation; (2) partial melting of crustal rocks. The Sangmelima region of the Congo craton is particularly interesting for the study of K-rich granitoid genesis because they outcrop in association with their supposed TTG protolith and at least one heat source for TTG protolith partial melting can be seen from field observations and geochronology. In this paper we present new geochemical and isotopic data of the Sangmelima high-K granitic group and demonstrate that they are of crustal origin, deriving from partial melting of TTG in late Archaean with doleritic magmatism as a major heat source.

Geological background

The Sangmelima region in Southern Cameroon constitutes the central north end of the Ntem complex (Shang et al. 2004a,b; Fig. 1), which represents the north-western part of the Congo craton in Central Africa (e.g. Bessoles and Trompette 1980; Maurizot et al. 1986). The Congo craton is a large sub-circular mass with a surface area of about 5.711.000 km^2 comprising Archaean basement, early to mid-Proterozoic fold belt and late Proterozoic cover (Goodwin 1991). It is bounded to the north by a major thrust that marks the contact with the Pan-African orogenic belt and is composed of various rock types. Most of it consists of the Archaean (2,825–2,900 Ma) TTG (comprising charnockites, granodiorites and tonalites; e.g. Nédélec et al. 1990; Shang et al. 2004a,b). Each of the three members of the TTG group comprises a suite of modally distinguishable rocks thought to have differentiated from three different TTG magmas by fractional crystallization (e.g. Nédélec et al. 1990; Shang 2001). The charnockites or orthopyroxene bearing granitoids are the oldest formation (2,900 Ma), while the granodioritic and tonalitic members are, respectively, 2,834 and 2,825 Ma old. These ages were constrained from TIMS zircon Pb–Pb and U–Pb geochronology and interpreted to represent emplacement ages (Shang 2001; Shang et al. 2004b; Shang et al. 2006; C. K. Shang et al., in preparation). In addition to the granitoids, the craton also contains a supracrustal rock sequence (metagraywakes, banded iron formations, sillimanite-bearing paragneisses and amphibolites, Fig. 1). They occur as disrupted belts up to several kilometers in length and as xenoliths in TTG (Fig. 2a, b), suggesting that they are older than the TTG (e.g. Nsifa et al. 1993; Shang 2001). Major migmatitic corridors crosscut both the TTG and supracrustal formations. The TTGs also have abundant gneissic and migmatitic structures exhibiting evidence of partial melting (Nsifa and Riou 1990; Tchameni et al. 2000; Shang 2001). Late granites and syenites intrude the TTG (e.g. Kornprobst et al. 1976; Nédélec 1990; Tchameni et al. 2000 and 2001; Shang et al. 2001a, b), and therefore clearly postdate the main crustal forming episode in the region. Sangmelima high-K granites have been dated at 2,721 ± 4 Ma (Fig. 3a; Shang et al. 2006; C. K. Shang et al. in preparation). The occurrence of doleritic dykes is thought to represent the last recognizable magmatic activity in the Ntem complex (e.g. Toteu et al. 1994; Vicat et al. 1996). But it is interesting to note that dolerites in the Sangmelima region have a similar crystallization age (2,723 ± 3.3 Ma; Fig. 3b; C.K. Shang et al., in preparation) as the high-K granites.

Two major episodes of deformation and two reactivation episodes are noted in the Ntem complex. (1) The first deformation episode is characterized by vertical foliation, stretching and vertical lineation and isoclinal folds. These structural elements are correlated with successive emplacements of the mid-Archaean granitoids (Shang et al. 2004b), considered to be diapiric by Shang (2001) and Tchameni (1997). (2) The second major deformational event is marked by the development of sinistral shear planes of N0°–N45°E and of partial melting of TTG and of the supracrustal country rocks with the generation of various granites. This event is described as post-Archaean and post-charnockitic migmatization by Nsifa and Riou (1990) but is now thought to be late Archaean: 2,666 Ma (e.g. Tchameni et al. 2000) and 2,721 Ma (e.g. Shang et al. 2006; C. K. Shang et al. in preparation and this paper).

Later regional reheating is apparent from Rb–Sr and U–Pb data: (1) Initially, Rb–Sr whole rock data from Lasserre and Soba (1976) suggest recrystallization between 2,400 Ma and 1,800 Ma; more recently, Toteu et al. (1994) dated the peak of this metamorphism at about 2,050 Ma, using U–Pb zircon data on metamorphic rocks from the Nyong series; a similar Rb–Sr biotite age reported by Shang et al. (2004a), date this metamorphism at 2,064 Ma; the same authors equally reported an older Rb–Sr biotite age of 2,299 Ma; all these ages are the signature of the Eburnean orogeny, which suggests a third major episode in the Ntem complex. (2) The TTG group bears imprints of strong mylonitization and retrogression (especially at the thrust contact with the Mbalmayo-Bengbis

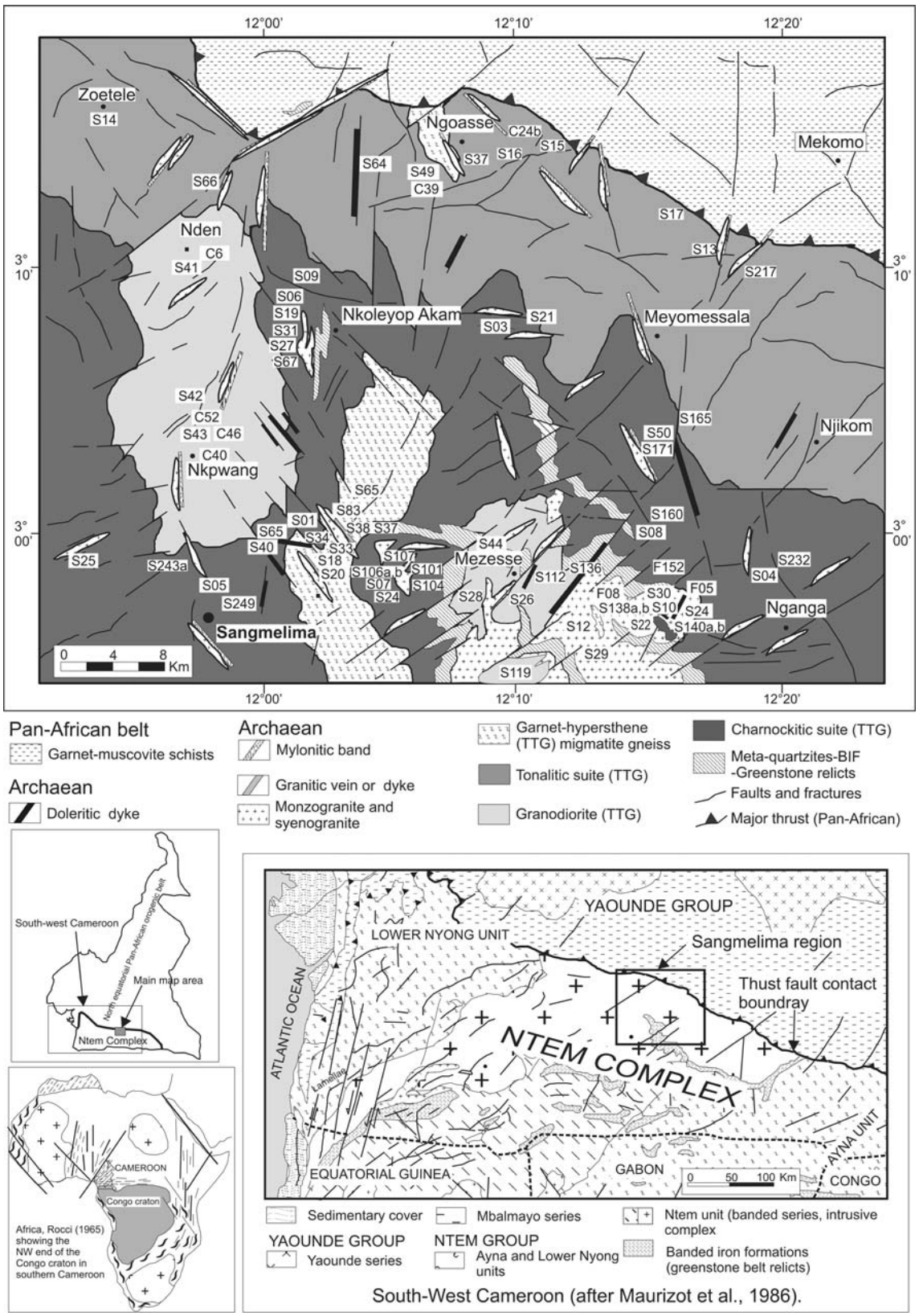

Fig. 1 Geological map of the north-western part of the Congo craton (Ntem complex) and thrust contact with the North Equatorial Pan-African orogenic belt (Yaounde group) in Southern Cameroon. *Main map* shows the geology of the Sangmelima region and localization of studied samples

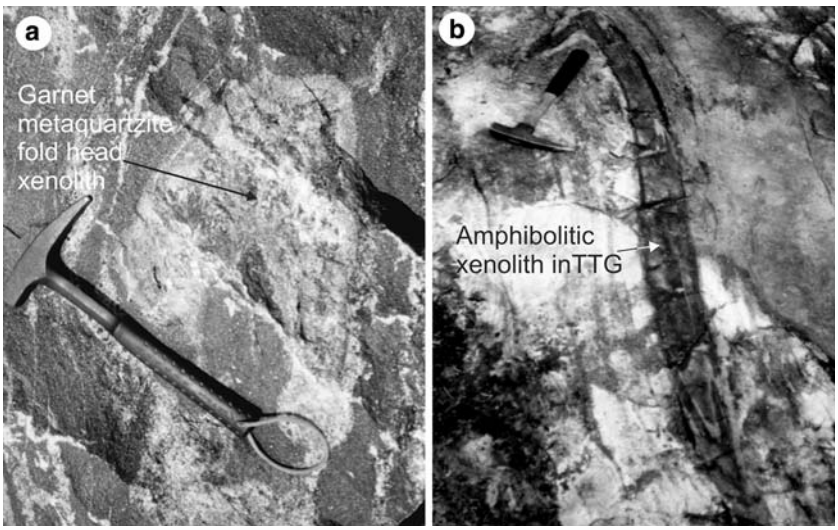

Fig. 2 Field pictures; **a** Folded metagreywacke xenolith in TTG that probably is the source of more radiogenic Sr in TTG granitic melts. **b** Amphibolitic xenolith in TTG that could have locally yielded low radiogenic Sr signatures in TTG melts

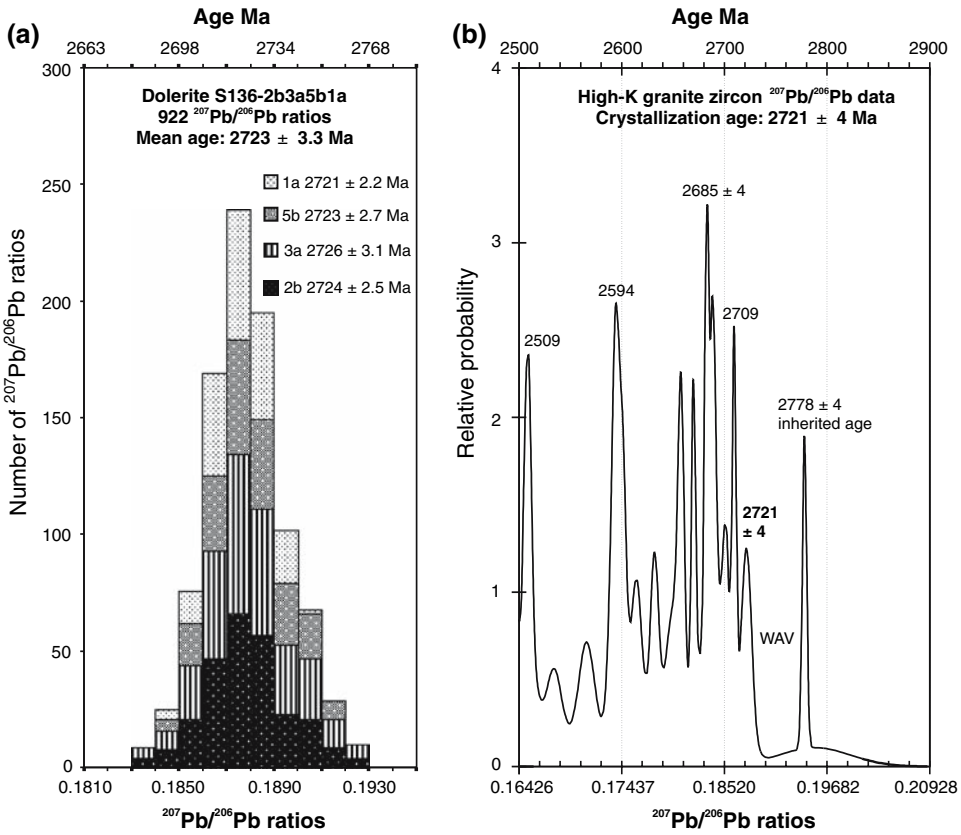

Fig. 3 Geochronological comparison of dolerites and high-K granites in the Sangmelima region. **a** Zircon evaporation Pb–Pb histogram taken from C. K. Shang et al. (in preparation), showing dolerite crystallization age (2,723 ± 3.3 Ma). **b** Relative probability plot of zircon evaporation Pb–Pb data, showing the crystallization age (2,721 ± 4 Ma) of high-K granites as well as an inherited age and a series of ages depicting various degrees of zircon Pb loss. WAV = 'wide age vacuum' between crystallization and inherited ages

schistose series), interpreted as Pan-African collision-metamorphism imprints; indeed, zircon U–Pb lower intercept Pan-African ages on charnockitic and granodioritic TTG of the Sangmelima region-Ntem complex reported by Shang et al. (2004b), indicate that the Pan-African orogeny has more intensively affected the northern margin of the Congo craton than hitherto thought.

Petrography

The granitoids of the Sangmelima region comprise three rock suites of the TTG group (charnockitic suite, granodioritic suite, tonalitic suite) and the high-K granitic group (Fig. 4). The rock suites occur principally with gradational or intrusive contacts in massifs, exhibiting compositional heterogeneities due probably

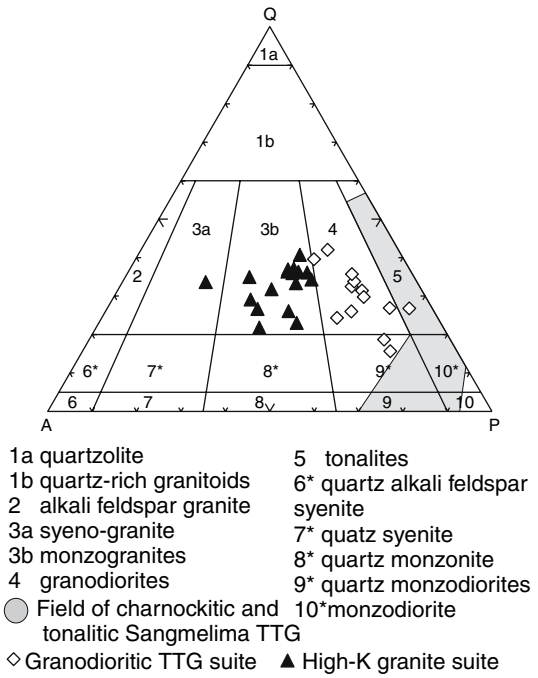

Fig. 4 Mesonorm module Q-A-P plot of Le Maitre et al. (1989) showing various members of the Sangmelima TTG and of the granitic groups

to magmatic differentiation. In all the rock types, reddish-brown to greenish biotite occurs as subhedral, 1–3 mm flakes often in association with subhedral feldspars, defining flow foliation. Alternating mesocratic and leucocratic banding accentuated by granitic lenses and schlieren in rocks affected by partial melting further define rock foliation. Mineral grains vary between 0.1–0.5 mm and attain 2–4 mm in coarse facies, defining granular texture with nematogranoblastic or granoclastic tendencies in oriented rock near shear corridors. In deformed rocks, the texture becomes heterogranoblastic with nested quartz and shows protomylonitic features characterized by polygonized quartz. A second generation of recrystallized interstitial plagioclase and quartz microblasts, rim the primary porphyroblastic phases. Accessories include zircon, apatite, ilmenite and magnetite.

The charnockitic suite ranges in modal composition from fine-medium grained norites to medium-coarse grained felsic enderbites, charnoenderbites and charnockites sensu stricto. They are dark grey to dark brown with bluish quartz lustre (due to inclusions) and malgachitic feldspars. Norites commonly display cumulate textures. Two mineral parageneses are identified in these rocks. The main mineral phases consist of subautomorphic hypersthene (the characteristic mineral that distinguishes the charnockitic suite from other rock types) and clinopyroxene, reddish-brown biotite, brown hornblende, antiperthitic An_{17-32} plagioclase and interstitial quartz. The second paragenesis is composed of green hornblende-actinolite and biotite in corona around pyroxenes, biotite–leucoxene on Fe–Ti oxides, and epidote and sericite after feldspars.

The tonalitic suite comprises three facies: leucocratic and coarse grained trondhjemite, mesocratic–melanocratic and medium grained diorite and meso-leucocratic medium grained tonalite. Nodule-like diorite with cumulate texture represents an early crystallized member of the rock suite. Amphibole preferentially defines localized magmatic flow foliation. Essential minerals include subhedral plagioclase (commonly An_{16-22}, with An_{27-28} in dioritic cumulates and albite (An_{7-10}) in trondhjemitic facies), microcline and quartz, in association with minor biotite, brown and green hornblende and relic clinopyroxene in mesocratic and melanocratic facies. Coronitic association of reddish brown biotite, Fe–Ti oxides and quartz around brown hornblende phenocrysts is observed in the dioritic facies. Chlorite and epidote are secondary phases after biotite and feldspars, respectively.

In the granodioritic suite massifs, granodiorite forms the main coarse to medium grained rock type. Other members of the suite include localized medium-grained darker nodules and lenses and layers of quartz monzodiorite and medium- to fine-grained leucocratic trondhjemite. Biotite often occurs in symplectitic associations with quartz and Fe–Ti oxides and forms inclusions in other mineral phases. It is important to note that biotite–quartz symplectitic association is a common texture in charnockites that have been hydrated: Opx + Kspar + H_2O = biotite + quartz. This suggests that some of the granodiorite could have first crystallized as charnockites. The more tonalitic and dioritic members of the granodioritic suite contain cumulate plagioclase, hornblende and pyroxene crystals. Minor clinopyroxene and brown hornblende blobs (0.4–1.4 mm) coexist with green hornblende and Fe–Ti oxides. Oligoclase (An_{12-20}) occurs as subhedral to anhedral antiperthitic-poikilitic laths. Microcline is the principal K-feldspar. It is often perthitic and also poikilitic. Quartz varies from 20 to 30%.

In the high-K granitic group, the light grey coarse to medium grained monzogranite is the main rock type. Syenogranite occurs as 1–2 m reddish medium to fine grained pods. The more pinkish monzogranite and syenogranite always show gradational or intrusive contacts. Rocks of this suite also occur as 1–5 cm aplitic veins, 1–4 dm and >1 m thick granitic and pegmatitic dykes crosscutting the gneissic country-rocks and charnockitic and granodioritic TTG massifs (Fig. 5b, c). The association of granitic material, in charnockitic and

gneissic massifs, with restitic melanocratic schlieren, gives an impression of a migmatitic assemblage due to partial melting. Granitic material also lodges in slits along shear corridors or are parallel to the foliation network of the host rock (Fig. 5a) or occurs as lenses with characteristic flame tongue forms (Fig. 5d). Pinkish microcline often phenocrystic and perthitic is the characteristic feldspar while plagioclase is less abundant and albitic (An_{3-8}). Plagioclase with slightly higher anorthite compositions ($An_{9.7-10.4}$) is noted mainly in granite lenses from charnockitic massifs. Intergrowths defining a vermicular texture myrmekite, often occur at the contact between quartz and plagioclase. Red-brown biotite is the principal ferromagnesian mineral but discrete more or less altered clinopyroxene and green hornblende are locally present.

Analytical techniques

Major and trace element analyses

Major and trace elements (Ba, Cr, Nb, Ni, Rb, Sr, V, Y, Zn, Zr) were analysed by X-ray fluorescence (XRF) on fused powder discs at the University of Tuebingen. Loss on ignition (LOI) was determined after igniting 1 g of rock sample powder in quartz crucibles at 1,050°C for 1 h. Analytical uncertainties are less than 1% for major elements and between 2 and 5% for trace elements. Other trace elements including (REE, Hf, Ta, W, Pb, Th, U) were analyzed by inductively coupled plasma mass spectrometry (ICP-MS) at the laboratory of the Africa Museum, Tervuren, Belgium. Analytical uncertainties are <10%.

Rb–Sr and Sm–Nd analyses

Isotope ratios have been measured at the University of Tuebingen. About 50 mg of whole-rock sample powder were spiked with mixed ^{84}Sr–^{87}Rb and ^{150}Nd–^{149}Sm tracers prior to dissolution in HF acid at 180°C and under high pressure in poly-tetrafluor-ethylene (PTFE) reaction bombs. Element separation (Rb, Sr and REE) was performed in quartz columns containing a 5 ml resin bed of AG 50W-X12, 200–400 mesh, conditioned and equilibrated with 2.5 N HCl. For Sm and Nd separation, 1.7 ml Teflon powder coated with di-ethyl hexyl phosphate (HDEHP) as cation exchange medium

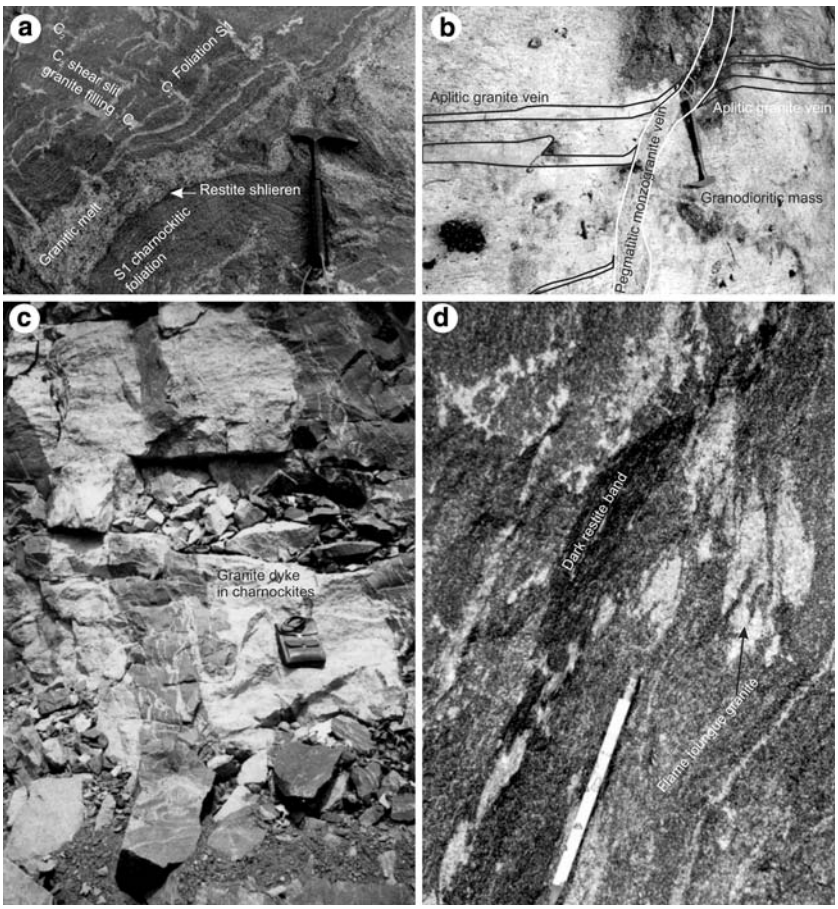

Fig. 5 Field-outcrop photographs: **a** granitic leucosome melt parallel to S_1 foliation and as infillings in slits parallel to C_2 microshears and perpendicular to S_1 foliation and dark restite bands; **b** pegmatitic and aplitic granite veins cut-crossing massive TTG; **c** metric granitic dyke cut-crossing a charnockitic massif in Nkoleyop-Akam area; **d** leucosomic granite flame tongue injections and a thick ferromagnesian restite band in a a charnockitic massif

was employed in smaller quartz columns, equilibrated with 0.18 N HCl. For mass spectrometric analyses, Sr was loaded with a Ta–HF activator and measured on a single W filament. Rb was loaded as a chloride and Sm and Nd were loaded as phosphates and measured in a double Re-filament configuration mode. All analyses were performed using a Finnigan MAT 262 thermal ionisation mass spectrometer (TIMS) equipped with 8 Faraday cups in a static collection mode. The $^{87}Sr/^{86}Sr$ ratios were normalized to $^{86}Sr/^{88}Sr = 0.1194$, the $^{143}Nd/^{144}Nd$ ratios to $^{146}Nd/^{144}Nd = 0.7219$, and Sm isotopic ratios to $^{147}Sm/^{152}Sm = 0.56081$. Analyses of 24 separate loads of Ames metal, (Geological Survey of Canada, Roddick et al. 1992), during the course of this study, gave a $^{143}Nd/^{144}Nd$ ratio of 0.512125 ± 10 (± 2σ error of the mean) and within the same period, the NBS 987 Sr standard yielded $^{87}Sr/^{86}Sr$ ratio of 0.710259 ± 12 ($n = 28$). Total procedural blanks (chemistry and loading), were <200 pg for Sr and <30 pg for Nd. Nd-model ages and ε_{Nd} were calculated using present day CHUR values of 0.1967 for $^{147}Sm/^{144}Nd$ (Jacobson and Wasserburg 1980) and 0.512638 for $^{143}Nd/^{144}Nd$ (Goldstein et al. 1984). Model ages were also determined using depleted mantle values as given in Liew and Hofmann (1988). Decay constant for ^{87}Rb (1.42×10^{-11} a^{-1}) was taken from Steiger and Jäger (1977) and for ^{147}Sm (6.54×10^{-12} a^{-1}) from Lugmair and Marti (1978).

Results

Major elements

The TTG group is characterized by a range in wt% SiO_2 from 53–77% (charnockitic suite, 54–70%; tonalitic suite, 58–77%; granodioritic suite, 62–73% with a remarkably low value of 53% for a dioritic member), in contrast to the high-K granitic group that shows a narrower SiO_2 range in wt% of 66–77%. Except for elements linked to feldspar (K_2O, Ba, Sr) and Zr, major and trace elements correlate negatively with increasing SiO_2 (Fig. 6). The data define near linear trends, suggesting that the primary mineral assemblage did not undergo important changes during fractionation. Cumulate textures and the close spatial field association of the various rock suite members indicate that they are linked through differentiation from the same magma.

All high-K granitic group members are peraluminous ($1.00 < (A/CNK) < 1.16$); aluminium saturation index (ASI), ($A/CNK = [Al_2O_3/(CaO + Na_2O + K_2O)$ mol%]). In contrast the TTGs are both metaluminous and peraluminous (granodioritic suite, $0.65 < (A/CNK) < 1.08$; tonalitic suite, $0.90 < (A/CNK) < 1.1$) except for the charnockitic suite that is metaluminous ($0.56 < (A/CNK) < 0.99$) but for one member (Fig. 7). The ASI tends to systematically increase with increasing SiO_2 (Table 1).

The most consistent major element difference between the two rock groups is alkali content; unsurprisingly, K_2O and K_2O/Na_2O are higher in granites while Na_2O and Na_2O/K_2O are higher in the TTGs (Fig. 8a, b). The TTG group is also generally more calcium rich and shows a tendency for Na as opposed to K enrichment during differentiation (Fig. 9b, c). In the normative An–Ab–Or diagram (Fig. 9a) used for rocks with >10% normative quartz (O'Connor 1965), the TTGs plot within a range which is typical of Archaean juvenile crustal rocks whatever their age and geographical origin (e.g. Barker 1979; Glikson 1979; Condie 1981), while members of the high-K granitic group essentially plot in the granite field. In the SiO_2 (wt%) versus $Na_2O + K_2O$–CaO plot (Fig. 9d), the TTG form a trend that spans the calcic and calc-alkalic domains. The plot of the granodioritic suite is similar to Archaean tonalitic gneisses. They also show features of both the A-type and cordilleran granitoids (e.g. Frost et al. 2001). In contrast, the high-K granitic group with a potassic calc-alkaline affinity (Fig. 9c) does not show a trend as members span the calcic, calc-alkalic, alkali-calcic and alkalic fields (Fig. 9d).

The TTGs have a high mafic content ($Fe_2O_3 + MgO + TiO_2 = 7.5–18\%$, except for some trondhjemitic samples 2–7%) as compared to the high-K granites (1.6–3.9%) but both rock groups have similar Mg# ($[Mg^{2+}/(Mg^{2+} + Fe_{Total}) \times 100]$, with Fe_{Total} as Fe^{2+}) ranges (TTGs, 32–60; high-K granites mostly 25–61; Table 1). In the SiO_2 (wt%) versus $FeO_{total}/(FeO_{total} + MgO)$ plot (Fig. 10a), the TTGs and high-K granites exhibit both magnesian and ferroan compositions, but it is interesting to note that the granodioritic suite is only magnesian.

Trace elements

Ni, Cr, V and Zn concentrations exhibit a negative correlation with increasing silica (Table 1; Fig. 6). The TTG group is enriched in Cr, Sr, V, Zn, Ni and Zr, and depleted in Ba, Rb and Y compared to the high-K granitic group. Nb shows a similar average abundance and also generally very low concentrations in all the rock types. K/Rb ratios vary between 144 and 942, giving high average values for TTGs (charnockites, 420; tonalites, 393; granodiorites, 371) compared to a low average value of 321 for the high-K granites.

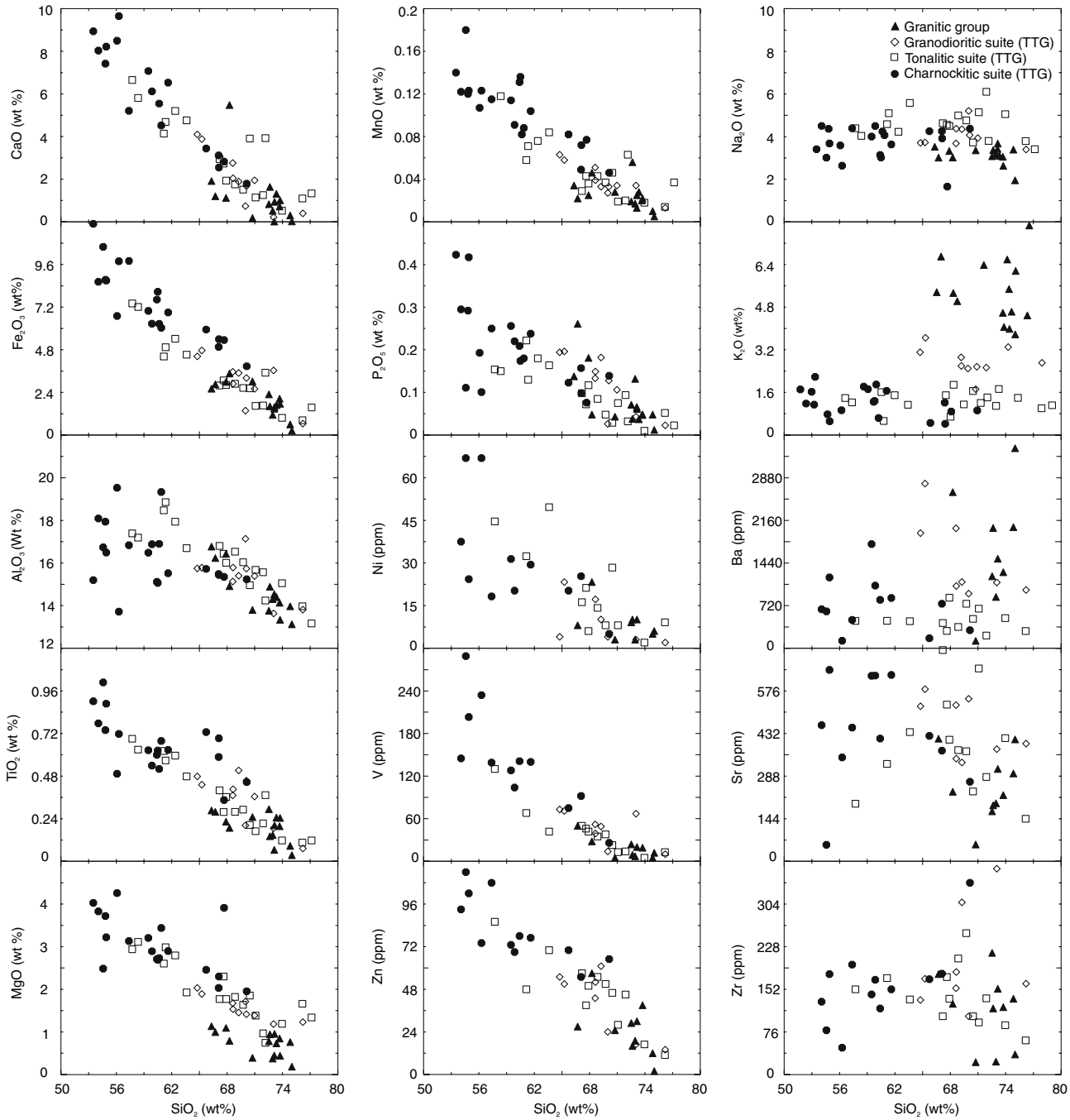

Fig. 6 Harker diagrams for selected major and trace elements. Oxides of Al, Ca, Fe, Mg, Mn, P, Ti and trace elements (Ni, V and Zn) portray a negative correlation with increasing SiO_2. No distinctive pattern is seen in the case of K_2O and Na_2O, Ba, Sr and Zr

Conversely, Rb/Sr ratios are quite low for TTGs (granodiorites, 0.08–0.28; charnockites, 0.01–0.78, except for sample S40, 1.66; tonalites 0.02–0.34) compared to high-K granites (0.14–1.64). Y versus Sr/Y plot (Fig. 10b) exhibit slab- and mantle-like compositions, while HFSE (e.g. Hf versus Zr; Fig. 9c; Hf/Zr = 40) indicate similar average ratios to MORB and chondrite (37 ± 2; e.g. David et al. 2000, and references therein). Good correlations are also observed between K–Ba, K–Rb and CaO–Sr (Figs. 10d, e, f).

Primordial mantle normalized spider diagrams (Fig. 11a) show generally similar patterns between TTGs and high-K granites, with negative Nb and Ti anomalies and positive La and Ce (LREE) and Y

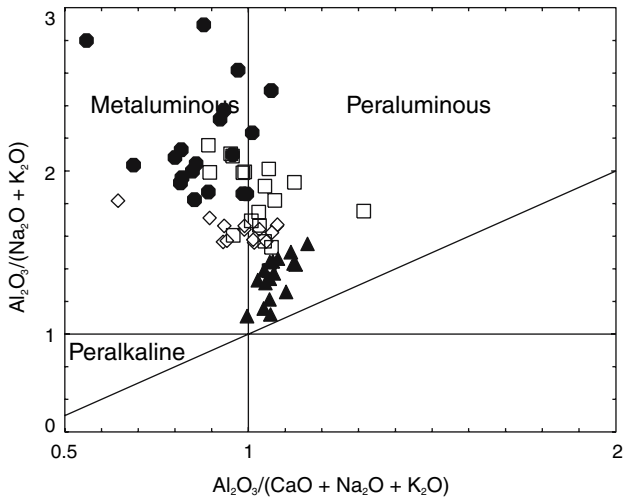

Fig. 7 Shand's Index (Maniar and Piccolli 1989), showing mainly metaluminous composition for charnockitic TTG, both metaluminous and peraluminous compositions for granodioritic and tonalitic TTGs and basically peraluminous composition for high-K granites. Legend as in Fig 5

anomalies. Variably positive and negative Ba, Th, Nd, anomalies occur in both rock groups. Comparatively low Th/U ratios (0.4–16) mark the TTGs while high ratios (1.8–95) characterise the high-K granites. The singularly high ratios observed in some samples in both groups are due to very high Th concentrations (Table 2). The primordial mantle normalized diagrams show that at similar SiO_2 content, the high-K granitic group has higher concentrations of most incompatible elements (except HREE) than the TTG group.

The TTGs display gentler and more or less parallel REE patterns with La_N/Yb_N ratios ranging from 18.8 to 99.7 (Table 2), except for sample S21 which is strongly depleted in HREE and shows a steeper pattern. The high-K granites exhibit steeper patterns (La_N/Yb_N ratios 12.2–53) but for sample S26 (Fig. 11b). However, LREE degree of fractionation is similar for both rock groups ($4.6 < La_N/Sm_N < 18.1$ for TTGs; $5.7 < La_N/Sm_N < 14.2$ for high-K granites) and the marked difference concerns the HREE ($2.3 < Gd_N/Lu_N < 5.1$ for TTGs; $1.2 < Gd_N/Lu_N < 17.3$ for high-K granites). TTGs have low total REE abundances (36 and 236 ppm) compared to high-K granites (75–538 ppm). In both rock groups, samples with low total REE abundances exhibit strong positive Eu anomalies (Eu/Eu* = 1.6–4.8 for TTGs and Eu/Eu* = 1.96 and 6.91 for high-K granites) that are probably due to high plagioclase or potassic feldspar content. On the other hand, negative anomalies are lower for high-K granites with high total REE abundances (Eu/Eu* = 0.57, 0.52, 0.24) compared to TTGs (Eu/Eu* = 0.6 and 0.9). Some siliceous members in both the TTG and high-K granitic groups with the lowest total REE abundance and Zr (e.g S21 and S67, respectively) show strong depletion in HREE with near typical Archaean TTG pattern. Their REE patterns probably reflect extraction of REES from the melt during zircon crystallization. Alternatively, they could be melts from a garnet rich source. Sample S26 of the high-K granitic group is more enriched in HREE, displaying a gentle slope similar to that of some members of the TTG group (Fig. 11b). These enriched patterns probably indicate the presence of zircon that concentrate HREEs or may be signatures of garnet free sources.

Sm–Nd and Rb–Sr isotope systematics

Sm–Nd and Rb–Sr isotope whole rock data are presented in Table 3. Initial Nd and Sr isotope ratios were calculated for the following TTG age values: 2,900 Ma for charnockites, 2,834 Ma for granodiorites, 2,825 Ma for the tonalites (e.g. Shang et al. 2004b) and 2,721 Ma for high-K granitic group (e.g. Shang et al. 2006; C.K. Shang et al., in preparation) and also for all TTGs for comparison. In the TTG group, $\varepsilon_{Nd,\2,900\ Ma}$ and the initial $^{87}Sr/^{86}Sr$ ($Sr_{i,\2,900\ Ma}$) ratios vary between 0.30 to –2.61, and 0.70126 to 0.70262, respectively for the charnockitic suite; while $\varepsilon_{Nd,\ 2834\ Ma}$ and the initial $^{87}Sr/^{86}Sr$ ($Sr_{i,\2834\ Ma}$) ratios vary between 0.3 to –1.65, and 0.70115 to 0.70206, respectively for the granodioritic suite and $\varepsilon_{Nd,\2,825\ Ma}$ and the initial $^{87}Sr/^{86}Sr$ ($Sr_{i,\2,825\ Ma}$) ratios vary between –0.71 to –3.45, and 0.70128 to 0.70318, respectively for the tonalitic suite. In the high-K granitic group, $^{87}Sr/^{86}Sr_{i,\2,721\ Ma}$ ratios vary between 0.70036 and 0.70687 and $\varepsilon_{Nd,\2,721\ Ma}$ values range from –2.45 to –5.31. At 2,721 Ma, the TTG group has similar $\varepsilon_{Nd,\2,721\ Ma}$ (–1.40 to –4.86) and low $Sr_{i,\2,721\ Ma}$ (0.70146–0.70348) to the high-K granitic group except for one member (Fig. 12a, b). Nd model ages (T_{DM} and T_{CHUR}) are similar for the TTGs (3,050–3,280 Ma; 2,832–3,185 Ma, respectively) and high-K granitic groups (3,130–3,310 Ma; 2,875–3,117 Ma, respectively) (Table 3; Fig. 13).

Discussion

Petrogenetic considerations

A brief look at the TTGs

The negative anomaly in Nb, Ti (Fig. 11b) and Ta (not shown) suggest a subduction process during or

Table 1 Major and trace element concentrations for Sangmelima granitoids: major elements are in weight per cent but for K which like trace elements is in parts per mil (ppm)

Charnockitic TTG	1	2	3	4	5	6	7	8	9	10	11	12	13	14	15	16	17	18	19
Sample	S107	S07	S40	S101	S06	S152	S10	S03	S83	S01	S05	S08	S160	S249	S138b	S09	S106b	S04	S232
SiO_2	53.6	54.1	54.6	54.8	54.9	56.1	56.3	57.4	58.7	59.5	59.9	60.4	60.5	60.7	60.9	61.6	63.5	65.7	67.1
TiO_2	0.9	0.8	1	0.74	0.89	0.49	0.72	1.3	0.54	0.63	0.54	0.6	0.62	0.52	0.68	0.63	0.51	0.73	0.69
Al_2O_3	15.2	18.1	16.7	18	16.5	19.5	13.7	16.8	15	16.5	16.9	15.1	15.1	16.9	19.3	15.5	15.8	15.7	15.4
Fe_2O_3	11.9	8.6	10.6	8.7	8.7	6.7	9.8	9.8	8.9	7	6.3	7.6	8.1	6.3	6	6.9	5.1	5.9	5.4
MnO	0.14	0.12	0.2	0.12	0.12	0.11	0.12	0.12	0.14	0.11	0.09	0.13	0.14	0.08	0.08	0.1	0.07	0.08	0.07
MgO	4.5	4	6.6	3.7	4.1	4.3	4.8	2.6	4.9	3.5	3.1	5.7	5.6	2.8	2.3	3.3	2.8	1.7	1.3
CaO	8.1	7.7	5	7.4	6.4	8.5	10.8	6.3	7.6	6.4	5.8	5.4	5.4	5.5	6.9	5.8	4.9	4.9	4.6
Na_2O	3.4	4.5	3	4.5	3.7	3.6	2.6	4.4	3	4	4.5	3.2	3	4.3	4.1	3.6	4.1	4.3	3.9
K_2O	1.7	1.2	1.6	1.14	2.2	0.78	0.52	0.93	1.2	1.8	1.7	1.3	1.3	1.9	0.64	1.7	2.6	0.45	0.42
P_2O_5	0.42	0.3	0.11	0.29	0.42	0.19	0.1	0.25	0.1	0.26	0.22	0.21	0.17	0.22	0.18	0.24	0.18	0.12	0.1
LOI	0.15	0.41	0.6	0.46	0.72	0.62	0.16	0.1	0.04	0.41	0.57	0.4	0.36	0.44	0.14	0.16	0.53	0.18	0.54
Total	99.9	99.9	100.2	99.8	98.9	100.9	99.8	100.2	100.1	100.4	99.7	100.3	100.3	99.5	101.2	99.7	100.1	100	99.6
Na+K	5.1	5.7	4.6	5.5	5.9	4.4	3.2	5.3	4.2	5.8	6.2	4.4	4.3	6.2	4.7	5.3	6.7	4.7	4.3
Na/K	2	3.8	1.9	3.8	1.7	4.6	5.1	4.7	2.5	2.2	2.6	2.5	2.4	2.2	6.4	2.2	1.6	9.4	9.3
Ab/An	1.5	1.5	1.1	1.5	1.4	0.9	0.9	1.2	1.1	1.6	1.8	1.1	1.1	1.8	1.1	1.4	2.2	1.6	1.6
A/CNK	0.69	0.8	1.1	0.82	0.82	0.88	0.56	0.86	0.75	0.82	0.86	0.93	0.93	0.89	0.97	0.85	0.86	0.96	99.6
Mg#	42	48	55	46	48	56	49	35	52	50	49	60	58	47	43	48	52	36	32
Ba		659	626		1197		129	479		1760	1058	818				850		169	
Cr		52	157		50		139	239		91	38	440				60		19	
K		9,819	13,479		18,111		4,283	7,736		15,073	14,309	10,383				13,761		3,768	
Nb		4	6		6		15	7		2	2	4				2		3	
Ni		37	66		24		66	18		31	20	74				29		20	
Rb		23	93		77		9	14		31	34	38				60		4	
Sr		460	56		647		351	452		627	628	415				630		424	
V		145	289		203		234	139		128	104	141				140		75	
Y		16	28		21		16	22		14	14	15				12		7	
Zn		93	114		102		74	108		73	69	78				77		70	
Zr		130	79		179		48	196		143	169	118				152		170	

Table 1 continued

Charn-ockitic TTG	20	21	22	Tonalitic TTG	2	3	4	5	6	7	8	9	10	11	12	13	14	15	16
Sample	S25	S138a	S12	S49	C39	S15	S171	C24b	S14	S13	S50	S64	S18	S20	S33	S66	S17	S165	S16
SiO_2	67.1	67.9	70.1	57.7	58.4	61.1	61.4	62.3	63.6	67.2	67.6	67.9	68.9	69.8	70.5	71.1	71.9	72.6	74
TiO_2	0.59	0.35	0.45	0.69	0.63	0.62	0.56	0.6	0.48	0.4	0.28	0.36	0.28	0.29	0.21	0.17	0.21	0.37	0.12
Al_2O_3	15.5	15.4	15.2	17.4	17.9	18.5	18.9	17.9	16.7	16.8	16.4	16	16.5	16	15	15.7	15.6	14.2	15.1
Fe_2O_3	5	5.4	3.9	7.4	7.2	4.4	5	5.5	4.5	2.8	3.1	2.8	2.9	2.7	2.6	1.6	1.7	3.5	0.97
MnO	0.05	0.08	0.05	0.22	0.12	0.06	0.07	0.08	0.08	0.03	0.04	0.04	0.04	0.04	0.05	0.02	0.02	0.06	0.02
MgO	1.6	1.4	0.1	3.3	2.9	2.1	2.3	2.6	2.4	1.5	1.4	0.97	0.88	0.76	2	0.57	0.63	2	0.26
CaO	4.1	7.8	3.9	5.9	6.2	5.2	6	5.6	3.9	3.5	4.6	3.6	3.6	3.3	3.7	2.8	1.9	1.5	2.4
Na_2O	4.3	1.7	4.4	4.4	4.1	4.6	5.1	4.2	5.6	4.6	4.6	4.5	4.5	4.8	3.7	5.2	6.1	3.8	5.1
K_2O	1.2	0.89	0.92	1.4	1.2	1.6	0.5	1.5	1.1	1.5	0.69	1.9	1.2	1.7	1.2	1.4	1.1	1.7	1.4
P_2O_5	0.16	0.08	0.14	0.15	0.15	0.22	0.13	0.18	0.16	0.1	0.07	0.12	0.09	0.05	0.03	0.08	0.09	0.03	0.01
LOI	0.34	0.04	0.31	0.69	0.81	1.8	0.52	0.41	1.3	1.5	0.76	1.1	0.48	0.53	0.6	0.74	0.94	0.45	0.57
Total	99.9	100.7	100.4	99.4	99.8	100.3	100.4	100.9	100	100.1	99.6	99.4	100	99.9	99.6	99.5	100.2	100.3	99.9
Na+K	5.5	2.6	5.2	5.8	5.3	6.2	5.6	5.7	6.7	6.1	5.3	6.4	6.1	6.4	4.9	6.6	7.2	5.5	6.5
Na/K	3.5	1.9	4.7	3.2	3.3	2.9	9.6	2.8	4.9	3.1	6.7	2.4	4.4	2.9	3.1	3.7	5.6	2.2	3.6
Ab/An	1.8	0.5	1.9	1.6	1.3	1.6	1.7	1.5	2.7	2.3	1.7	2.2	2.4	2.5	1.7	3.2	5.6	4.7	3.5
A/CNK	0.98	0.86	0.99	0.9	0.93	0.99	0.95	0.96	0.96	1.1	0.99	1.01	1.03	1.02	1.1	1.04	1.1	1.3	1.1
Mg#	38	34	32	47	44	48	48	49	51	51	47	40	38	36	60	41	43	52	35
Ba	753		305	462		464			458	425	294	855	360	754	496	669	216		509
Cr	26		0	57		29			50	3	16	11	12	1	28	3	5		–
K	10,093		7,669	11,539		13,379			9,412	12,417	5,702	15,662	9,528	1,375	9,977	11,720	9,097		11,554
Nb	6		6	10		1			3	4	–	1	4	1	1	1	3		2
Ni	25		5	44		32			49	16	21	6	14	8	28	8	–		2
Rb	28		21	67		50			22	41	9	62	11	33	23	38	27		26
Sr	374		269	195		329			437	714	529	411	376	372	236	652	285		416
V	92		26	130		68			42	50	46	42	35	38	23	13	14		5
Y	8		10	28		8			21	2	3	7	8	6	2	1	3		3
Zn	55		65	86		48			70	57	39	50	55	51	46	28	45		17
Zr	180		342	152		172			134	104	174	135	207	252	104	93	136		88

Table 1 continued

Tonalitic TTG	17	18	Grandior. TTG	2	3	4	5	6	7	8	9	10	11	12	13	14
Sample	S38	S140a	C40	C46	S65	S42	C52	F05	S43	S44	S19	S41	S21	C6	S119	S27
SiO_2	76.2	77.2	52.6	62.4	64.9	65.3	66.4	67.2	68.6	68.6	68.9	69.3	70	70.1	71	73
TiO_2	0.11	0.12	0.79	0.49	0.48	0.43	0.26	0.3	0.37	0.41	0.28	0.51	0.2	0.45	0.37	0.19
Al_2O_3	14	132	15.4	17.5	15.8	15.8	17.4	16.5	15.1	15.8	16.5	15.4	17.1	15.7	15.4	13.6
Fe_2O_3	0.84	1.6	8.94	4.71	4.4	4.8	3.2	3.1	3.6	2.9	2.9	3.5	1.4	3.2	2.6	3.6
MnO	0.01	0.04	0.17	0.07	0.06	0.06	0.05	0.04	0.05	0.04	0.04	0.03	0.03	0.03	0.03	0.03
MgO	0.55	0.67	6.7	2.3	2.1	1.9	0.92	0.97	1.4	1.02	0.88	0.94	0.37	0.84	0.97	0.11
CaO	3.3	2.7	8.5	5.1	4.1	3.8	4.1	3.7	3.3	3	3.6	2.9	3.4	2.8	2.8	2.4
Na_2O	3.8	3.4	4.2	4.9	3.7	3.7	5.4	5.2	3.7	4.4	5	4.4	5.2	4.1	3.9	3.1
K_2O	1.01	1.1	1.5	2	3.1	3.7	2	1.2	2.9	2.6	1.2	2.5	1.7	2.6	2.5	3.3
P_2O_5	0.05	0.02	0.27	0.18	0.19	0.2	0.04	0.09	0.13	0.15	0.09	0.18	0.03	0.13	0.11	0.04
LOI	0.42	0.62	0.78	0.76	0.42	0.68	0.04	0.32	0.48	0.52	0.48	0.36	0.37	0.04	0.42	0.52
Total	100.3	100.6	99.9	100.6	99.3	100.7	99.9	98.7	100	99.7	100	100.2	100	100.4	100.1	100.2
Na+K	4.8	4.5	5.7	6.9	6.8	7.4	7.4	6.4	6.6	7	6.1	7	6.9	6.6	6.5	6.4
Na/K	3.8	3	0.36	0.41	0.84	1	0.37	0.23	0.78	0.59	0.24	0.57	0.33	0.63	0.64	1.06
Ab/An	1.9	2.3	1.9	2.1	1.8	2	2.6	2.5	1.9	2.5	2.3	2.6	2.5	2.6	2.5	2.2
A/CNK	1.1	1.13	0.65	0.89	0.94	0.93	0.94	0.99	0.99	1.01	1.06	1.02	1.03	1.08	1.08	1.05
Mg#	56	46	60	49	48	45	37	39	43	41	38	35	35	34	43	5.5
Ba	291		499	928	1944	2782	834	366	2026	1051	360	1122	924			1111
Cr	4		304	30.2	28	57	7	10	84	34	12	14	0			46
K	8,358		12,450	16,600	25,779	30,270	16,600	9,960	24,203	21,547	22,468	20,767	14,301	21,580	20,750	27,407
Nb	3		–	–	2	3	–	–	3	9	1	6	2			–
Ni	9		155	10	4	23	–	–	–	17	14	10	4			3
Rb	17		34	45	81	77	37	11	48	97	11	81	21			55
Sr	144		446	538	524	582	375	363	528	347	376	334	549			379
V	13		109	71	73	71	36	29	52	39	35	49	14			67
Y	1		35	13	10	11	–	–	4	10	8	6	1			12
Zn	11		116	57	55	51	48	52	43	52	55	61	24			17
Zr	61		115	189	133	171	96	227	154	183	207	307	104			367

Table 1 continued

High-K Granitic group	1	2	3	4	5	6	7	8	9	10	11	12	13	14	15	16	17
Sample	S243a	S24	S104	S34	S30	S29	S37	S22	S140b	S28	S112	S217	S26	S106a	S31	S67	F08
SiO_2	66.3	66.7	67.9	68.3	70.8	72.5	72.7	72.9	73.1	73.2	73.4	73.7	73.8	74.4	74.9	75	76.8
TiO_2	0.29	0.28	0.22	0.19	0.25	0.29	0.14	0.15	0.07	0.2	0.25	0.2	0.24	0.08	0.09	0.04	0.04
Al_2O_3	16.8	16.2	16.4	14.9	13.8	13.8	14.9	14.3	14.5	14.4	14.4	14.1	13.3	14.4	13.9	13.1	13.7
Fe_2O_3	2.6	2.9	3	3.5	3	2.3	1.6	1.1	1.5	1.6	1.7	2.1	1.8	1.1	0.6	0.3	0.4
MnO	0.03	0.02	0.03	0.05	0.03	0.02	0.06	0.02	0.01	0.03	0.03	0.02	0.02	0.02	0.01	0.01	0.01
MgO	0.96	0.6	0.56	2.7	0.09	0.41	0.82	0.26	0.01	0.47	0.66	0.36	0.5	0.54	0.15	0.01	0.12
CaO	2.3	2	2.2	1.6	0.8	1.6	1.9	0.8	0.9	1.9	1.5	1.7	0.9	2	1.5	0.4	1.5
Na_2O	3.5	3	3.3	3	3.4	3.1	3.4	3.2	3.4	3.7	3.1	3.1	2.6	3.2	3.4	2	3.5
K_2O	5.4	6.7	5.3	5	6.4	4.6	4.1	6.6	5.5	4	4.6	3.8	6.2	4.4	4.5	7.9	4.4
P_2O_5	0.14	0.26	0.18	0.05	0.04	0.07	0.04	0.13	0.07	0.06	0.04	0.05	0.05	0.03	0.05	0.01	0.02
LOI	0.78	0.79	0.46	0.31	0.46	0.73	0.51	0.35	0.42	0.37	0.32	0.66	0.33	0.58	0.32	0.29	0.37
Total	99.1	99.5	99.6	99.6	99.1	99.4	100	99.8	99.5	99.8	99.9	99.7	99.7	101	99.4	98.9	101.1
Na+K	8.9	9.7	8.7	8	9.7	7.7	7.4	9.8	8.9	7.7	7.7	6.8	8.8	7.6	7.9	9.8	7.9
K/Na	1.5	2.2	1.6	1.7	1.9	1.5	1.2	2.1	1.6	1.1	1.5	1.2	2.3	1.4	1.3	4	1.4
Ab/An	2.9	2.6	2.9	3.1	7.8	3.4	2.9	8.5	7.2	3.2	3.7	3.2	4.9	2.5	3.6	5.6	3.7
A/CNK	1.07	1.03	1.08	1.12	1	1.07	1.12	1.04	1.13	1.04	1.1	1.16	1.06	1.06	1.06	1.06	1.05
Mg#	42	29	27	61	6	26	50	31	1	37	43	26	36	50	33	7	38
Ba		6052		2637	126	1359	2032	866		1514			1427	2790	2059	3019	2459
Cr		0		7	0	0	6	0		5			0	0	40	0	0
K		55,610	44,239	41,666	52,954	38,014	33,615	54,697	45,484	33,034	38,429	31,291	51,128	36,188	37,267	65,238	36,603
Nb		2		3	5	3	4	2		3			9	0	6	1	0
Ni		8		23	3	9	10	3		10			0	0	5	6	0
Rb		128		90	555	129	68	322		152			246	83	118	186	98
Sr		414		235	57	169	189	196		312			224	584	297	412	286
V		50		38	5	24	9	7		20			19	24	5	12	9
Y		13		4	26	14	16	24		13			27	3	11	9	3
Zn		27		57	25	29	16	19		30			39	1	12	2	0
Zr		179		126	22	217	118	23		153			120	144	135	36	116

All trace elements concentrations are in ppm (–) not determined

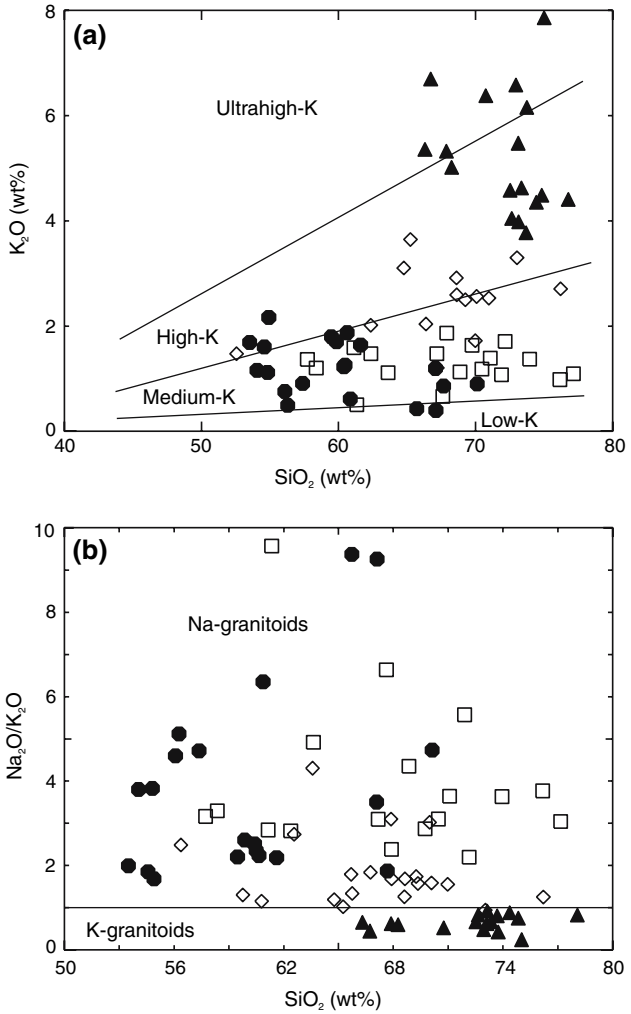

Fig. 8 **a** K_2O versus SiO_2 plot for Sangmelima granitoids with fields based on Gills (1981), showing high- to ultrahigh-K composition for Sangmelima granites as opposed to low- to high-K TTG composition and **b** Na_2O/K_2O versus SiO_2 plot; TTG plot in the Na-granitoid field while granite suite members plot in the K-granite field. Legend as in Fig. 5

before the generation of the TTGs. It is important to note that this geochemical signature in subduction zones is linked to the melting of subducted eclogite where rutile is a common restite phase that retains Nb and Ti. Noteworthy too is the fact that Nb and Ti negative anomaly is also observed in cases of overthickened oceanic crust, a common model for the generation of TTGs. T_{DM} model ages vary from 2,980 to 3,250 Ma (Table 3), being 146–286 Ma, 110–340 Ma, and 205–425 Ma older than the zircon crystallization ages for granodioritic, charnockitic and to tonalitic TTGs, respectively. This age disparity, that is similar to cases in modern plate tectonics with ocean floors of up to 200 Ma older than the subduction event, seems to be bigger than would be expected in Archaean rocks, given the rapid geodynamics due to then more numerous and smaller oceanic plates. These age differences in the Archaean Sangmelima TTGs could be ascribed to contributions of older sediments/crust during the remelting of the subducted slab that then produced older TDM model ages. T_{CHUR} ages vary from 2,832 to 3,180 Ma, being very similar, some only slightly older than the zircon ages. If these T_{CHUR} and zircon age similarities mean that TTG progenitors were derived from a CHUR mantle, then the progenitors were remelted only shortly after extraction from the mantle. In this regard, the T_{CHUR} model would fit better to the expected quick Archaean crust recycling than the depleted mantle model for Sangmelima TTG genesis.

The high-K granitic group

It is widely reported that calc-alkaline potassic rocks in Archaean granite-gneissic terranes are generally younger than the TTGs and are emplaced during late- to post-orogenic evolution of orogenic belts (e.g. Pitcher 1993), marking the late- to post-orogenic evolution of Archaean cratons (e.g. Jahn et al. 1987; Tchameni et al. 2000). In the field, the Sangmelima high-K granitic rocks clearly postdate the TTGs (Fig. 5a, b, c, d). Granite association with restite in a gneissic–migmatitic assemblage with TTGs suggests direct melting of the TTGs, generating granitic melts (e.g. Shang et al. 2001a, b). This rock association has been described as post-Archaean and post-charnockitic migmatization (e.g. Nsifa and Riou 1990; Nédéléc 1990). It is difficult to constrain the amount and conditions of TTGs melting at the formation of Sangmelima high-K granites but some known examples might give us an estimate. Many workers (e.g. Beard and Lofgren 1991; Rushmer 1991; Wolf and Wyllie 1994; Patiño Douce and Beard 1995) have shown that dehydration melting of mafic rocks between 800 and 1,100°C yields felsic melts with calc-alkaline composition. Some workers (e.g. Helz 1976) have proposed a smaller percentage melting of an amphibolitic source for the origin of silicic and potassic melts. But to reach the critical melt fraction of about 30–40% required for a felsic melt to separate from its source and define discrete magma bodies (e.g. Wickham 1987), temperatures in excess of 900°C would be required (e.g. Kampunzu et al. 2003). Such large proportions (~35–45%) of partial melting of the mafic lower crust have been estimated for the origin of California high-K felsic rocks (e.g. Tepper et al. 1993; Borg and Clynne 1998) of similar chemical composition to Sangmelima high-K granites.

The alkalic to calcic (Fig. 9d) and highly magnesian to highly ferroan (Fig. 10a) high-K Sangmelima gran-

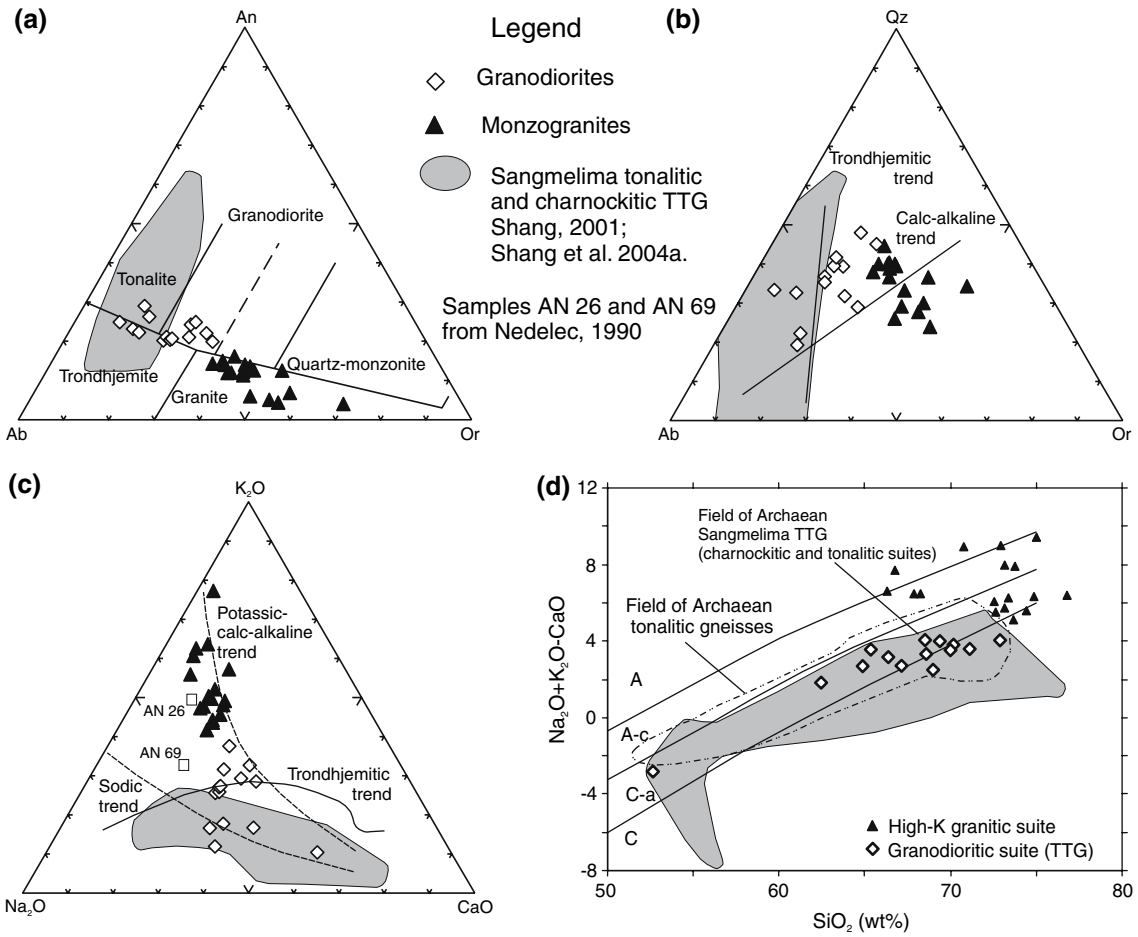

Fig. 9 **a** Plot of Sangmelima TTG and granite groups in the An–Ab–Or normative feldspar composition fields from O'Connor (1965) modified by Barker (1979) to account for K_2O present in biotite; **b** Normative Qz–Ab–Or diagram of Barker and Arth (1976) and **c** Na_2O–K_2O–CaO diagram with trends drawn by Luais and Hawkesworth (1994) and references therein exhibiting a trondhjemitic and a sodic trend for Sangmelima TTG group and a potassic calc-alakline affinity for the granitic group; **d** SiO_2 versus $Na_2O + K_2O$–CaO classification diagram after Frost et al. (2001), showing a trend in the calcic and calc-alkalic fields for Sangmelima TTG as opposed to the wide distribution from the calcic through calc-alkalic and alkali-calcic to alkalic fields for the granite group

ites in many ways behave like peraluminous leucogranites although some of its members are less siliceous than peraluminous leucogranites. They share partial features of A-type and cordilleran granitoids (e.g. Frost et al. 2001). Their chondrite normalised REE patterns are similar to those of Francistown high-K granites from NE Botswana (e.g. Kampunzu et al. 2003) and to calc-alkaline felsic rocks from modern continental active margins such as rhyolites and granites from the Cascades (e.g. Tepper et al. 1993; Borg and Clynne 1998).

The Eu anomaly variation (negative and positive; Fig. 11b) may indicate melting under low and high aH_2O, respectively. If the relatively high Y and Yb content of some samples and their almost flat pattern are suggestive of a garnet free source, then it is likely that partial melting was under low total pressure. Garnet is often absent in dehydration melting experiments conducted at less than 8 kbar (e.g. Rushmer 1991; Rapp et al. 1991). In this regard, some Sangmelima high-K granites could have been generated under such conditions within the middle of the crust. It is however interesting to note that garnet would appear at pressures >10 kbar (e.g. Wolf and Wyllie 1994) with ensuing implications. If this were the case, it could then be argued that low concentration in Ti and Yb and the high La_N/Yb_N Gd_N/Yb_N reflected in the steeper REE patterns (Fig. 11b) of some high-K granites could be due to a garnet rich residue (e.g. Kay et al. 1994; Mpodozis et al. 1995; Kay and Abbruzzi 1996). This argument notwithstanding, it must be made clear that only the most evolved granitoids (S21, 67) seem to

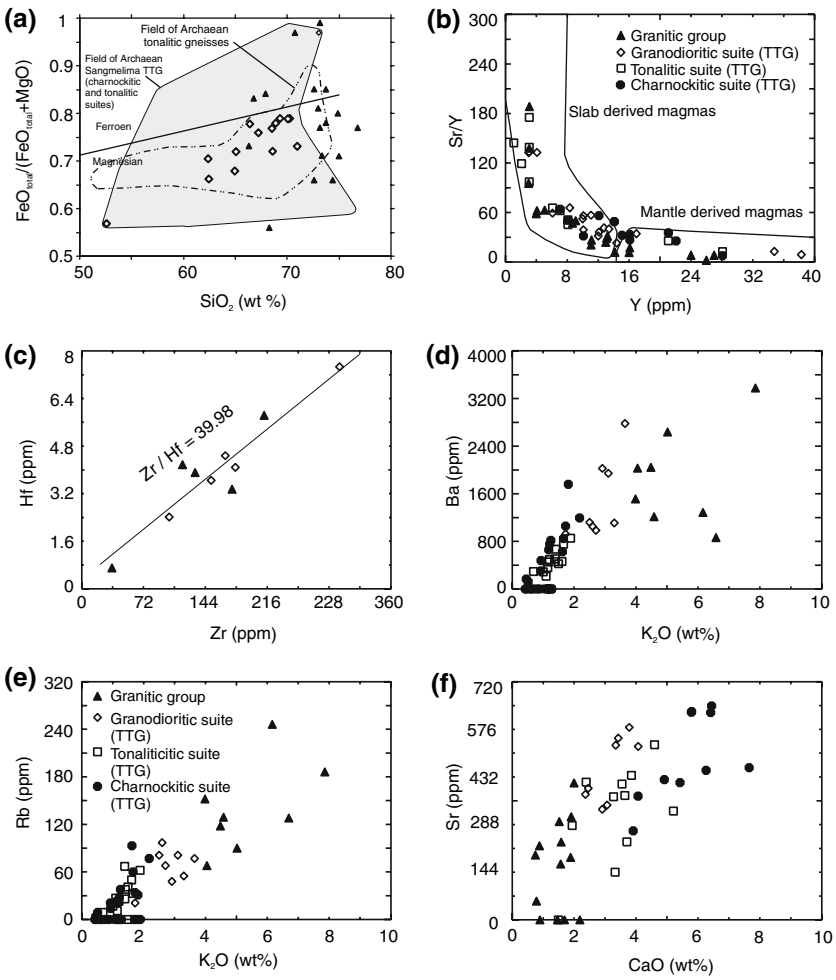

Fig. 10 More geochemical compositions of the Sangmelima granitoids in binary plots; **a** SiO_2 versus $FeO_{total}/(FeO_{total} + MgO)$, while charnockitic and tonalitic TTG as well as the granites portray both magnesian and ferroan compositions similar to the chemistry of Archaean tonalitic gneisses, granodioritic TTG show only magnesian composition. **b** Y versus Sr/Y diagram showing mantle- and slab derived-like composition of both TTG and granites. Granite chemistry is inherited from TTG that are effectively generated from mantle derived material. **c** High-field-strength-elements Hf versus Zr, showing good correlation and Zr/Hf MORB- and chondrite-like ratio. **d** Ba–K_2O, **e** Rb–K_2O, and **f** Sr–CaO good correlations

show REE patterns indicating garnet in the restite and the hook pattern typical of Archaean TTGs. In another consideration, some of the REE variations and the highest Eu anomalies could be reasonably ascribed to zircon crystallization.

Nature of the high-K granitic group parental magma and potential sources

Metabasic rocks have been cited as unsuitable sources for high-K granitoids because of their low K_2O contents (e.g. Roberts and Clemens 1993; Kampunzu et al. 2003), yet a granitoid suite that includes K-granites can be derived from amphibolites (e.g. Patiño Douce 1999; Fig. 14). Roberts and Clemens (1993) show that high-K granites are derived from partial melting of metamorphosed hydrous intermediate calc-alkaline rocks. Carroll and Wyllie (1989) in their experimental data indicate that partial melting of tonalites could produce high-K granite melts. Following the model of Querre (1985), the remelting of some TTG-like protolith in the lower crust can produce melts similar to Sangmelima high-K granites. Given the field relationship (e.g., Fig. 5a), and identical REE patterns (Fig 11b) as well as isotope data (Table 3; Fig. 13) between TTG rock formations and the high-K granites, we infer that TTG material represents the potential source of high-K granites in the Congo craton. In another critical note, Sangmelima high-K granites plot in the field of melts from metagreywackes as well as from mafic rocks (Fig. 14). This could be a reflection of the complex source composition with mafic and felsic (crustal) components input (e.g. Fig. 2; Nsifa et al. 1993; Shang 2001). It is, however, worth noting that metagreywackes usually have the assemblage quartz–plagioclase–biotite±hornblende which is similar to the assemblage of TTGs we imply in this study are protoliths to the granites; this fact could explain the similar composition of TTG derived granites to those derived from greywackes.

Assuming that the leucosome represents exactly the composition of the melt that was generated during protolith partial melting, we directly compared major and trace element composition of a leucosome granitic

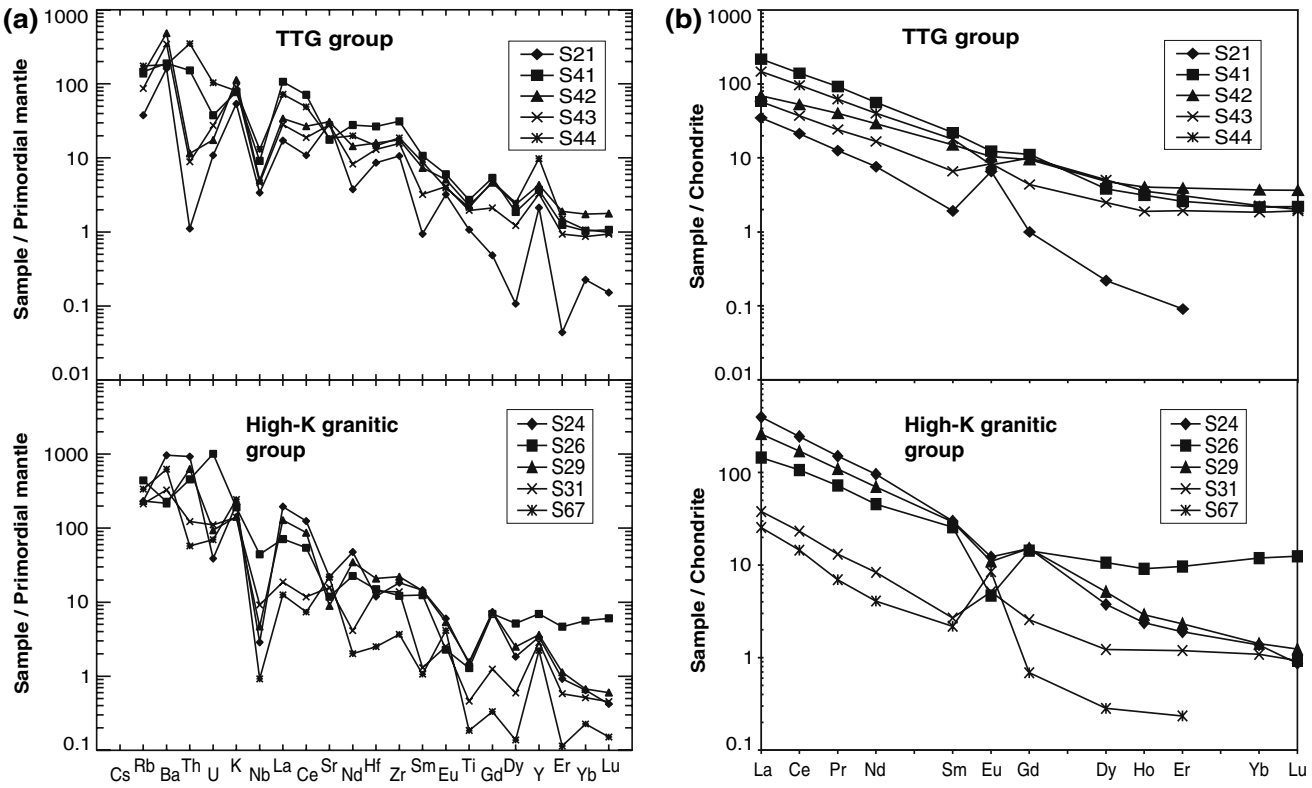

Fig. 11 **a** Primordial mantle normalized spidergrams (to the values of Sun and McDonough 1989). **b** Chondrite normalized REE patterns (to the values of Taylor and McLennen 1985) for selected samples of the Sangmelima TTG and granitic groups

Table 2 REE abundances (ppm) in Sangmelima granitoids

TTG group						Granitic group				
Sample	S42	S43	S44	S41	S21	S24	S29	S26	S31	S67
La	21.4	17.8	45.5	67.3	10.8	122.8	80.5	44.9	11.8	7.9
Ce	42.6	30	77.8	113	17.2	198.1	137.5	86.1	18.8	11.7
Pr	4.9	3	7.6	11.3	1.5	18.3	13.3	8.8	1.6	0.84
Nd	17.5	10	24.1	33.7	4.6	57.5	41.9	27.3	5	2.4
Sm	2.9	1.3	3.5	4.3	0.38	5.8	5.7	5	0.52	0.43
Eu	0.77	0.61	0.59	0.91	0.48	0.9	0.81	0.34	0.38	0.62
Gd	2.5	1.1	2.6	2.9	0.26	3.91	3.91	3.7	0.66	0.18
Dy	1.6	0.81	1.6	1.2	0.07	1.21	1.66	3.42	0.39	0.09
Ho	0.29	0.14	0.25	0.22	0.05	0.17	0.21	0.66	0.05	0.05
Er	0.82	0.4	0.65	0.54	0.02	0.4	0.49	2.02	0.25	0.05
Yb	0.77	0.38	0.47	0.46	0.1	0.29	0.3	2.49	0.23	0.1
Lu	0.12	0.06	0.07	0.07	0.01	0.03	0.04	0.4	0.03	0.01
Hf	4.5	3.7	4.1	7.5	2.4	3.4	5.8	4.2	3.9	0.7
Ta	0.05	0.05	0.6	0.15	0.05	0.05	0.05	8.55	0.45	0.05
W	0.66	0.58	0.51	0.99	6.5	0.5	0.81	1.07	0.7	0.41
Pb	15	14	21	13	12	43	31	33	17	24
Th	1	0.8	31	13	0.1	82	56	40	11	5
U	0.39	0.6	2.3	0.83	0.24	0.86	2.06	22.2	2.45	1.54
Σ REE	99.1	66.6	164.7	235.9	35.5	538.4	381.5	294.6	74.8	55.6
K/Rb	393	504	222	256	681	435	295	208	316	351
Rb/Sr	0.13	0.09	0.28	0.24	0.04	0.31	0.76	1.1	0.4	0.45
Th/U	2.6	1.3	13.4	16.1	0.4	94.9	27	1.8	4.4	3.3
La_N/Yb_N	18.8	31.3	72.9	99.7	72.6	285	181	12.2	34.6	52.9
Eu/Eu*	0.9	1.6	0.6	0.8	4.7	0.57	0.52	0.24	2	6.9

Table 3 Sm, Nd, Rb and Sr abundances and isotopic composition from Sangmelima granitic and TTG groups/suites

Sample	Sm (ppm)	Nd (ppm)	$^{147}Sm/^{144}Nd$	$^{143}Nd/^{144}Nd \pm 2\sigma_m$	εNd_{Ma}	$\varepsilon Nd_{2721\ Ma}$	$T_{DM/Ma}$ LH	$T_{CHUR\ Ma}$ LH	Rb ppm	Sr ppm	$^{87}Rb/^{86}Sr$	$^{87}Sr/^{86}Sr \pm 2\sigma_m$	Sr_{Ma}	$Sr_{2721\ Ma}$
Granitic group														
S24	6.926	66.14	0.0636	0.510072 (7)		–3.35	3,180	3,080	128	414	0.8976	0.742223 (10)		0.70686
S26	4.284	23.42	0.1106	0.510904 (8)		–3.69	3,190	3,110	239.7	209	3.3601	0.836486 (10)		0.70408
S29	6.637	53.54	0.0751	0.510327 (10)		–2.45	3,100	2,980	128.5	157.3	2.3836	0.794286 (10)		0.70036
S31	1.367	8.749	0.0944	0.510532 (7)		–5.31	3,320	3,270	118	297	1.1545	0.752360 (12)		0.70687
S67	0.336	2.581	0.0741	0.510289 (10)		–4.52	3,130	3,020	186	412	1.3124	0.756330 (10)		0.70462
Granodioritic suite (TTG)					$\varepsilon Nd_{2834\ Ma}$								$Sr_{2834\ Ma}$	
S21	0.509	4.558	0.0675	0.510137 (12)	–1.65	–3.56	3,120	3,010	17.2	501	0.0993	0.705376 (9)	0.7013	0.70146
S41	5.727	53.1	0.0651	0.510161 (9)	–0.33	–2.28	3,010	2,870	77.9	312.6	0.7226	0.730818 (10)	0.70115	0.70235
S42	3.282	20.35	0.0974	0.510739 (8)	–0.85	–2.32	3,050	2,920	73.2	554.9	0.3819	0.717524 (10)	0.70184	0.70248
S43	1.764	13.16	0.081	0.510432 (8)	–0.83	–2.54	3,050	2,920	45.1	497.2	0.2624	0.712375 (9)	0.7016	0.70204
S44	4.302	32.17	0.0808	0.510472 (8)	0.03	–1.68	2,980	2,832	94.3	325.1	0.8415	0.736627 (12)	0.70206	0.70347
Charnockitic suite (TTG)					$\varepsilon Nd_{2900\ Ma}$								$Sr_{2900\ Ma}$	
S03	6.153	29.78	0.1249	0.511277 (9)	0.26	–1.42	3,010	2,872	12.2	454.2	0.0775	0.704520 (9)	0.70126	0.70147
S04	1.284	6.27	0.1238	0.511258 (7)	0.3	–1.4	3,010	2,870	1.41	401.2	0.0101	0.702373 (13)	0.70195	0.70197
S06	6.82	36.85	0.1118	0.510955 (9)	–1.16	–3.15	3,180	3,020	80.9	647.9	0.3617	0.716648 (10)	0.70144	0.7024
S08	3.557	18.34	0.1172	0.511051 (8)	–1.3	–3.16	3,140	3,030	35.2	406.2	0.2505	0.712124 (7)	0.70159	0.70226
S10	2.047	7.15	0.1731	0.512142 (9)	–0.88	–1.43	3,100	2,990	4.64	350.4	0.0383	0.704234 (10)	0.70262	0.70273
S25	2.86	17.18	0.1006	0.510666 (10)	–2.61	–4.86	3,240	3,170	26.3	352.5	0.2163	0.711372 (10)	0.70228	0.70285
Tonalitic suite (TTG)					$\varepsilon Nd_{2825\ Ma}$								$Sr_{2825\ Ma}$	
S13	0.976	6.338	0.093	0.510670 (10)	–0.71	–2.12	3,030	2,900	34.6	662.3	0.1513	0.707469 (10)	0.70128	0.70151
S16	0.51	3.148	0.0979	0.510621 (30)	–3.45	–4.79	3,250	3,180	20.7	376.1	0.1593	0.707902 (10)	0.70138	0.70163
S17	1.578	10.89	0.0876	0.510472 (14)	–2.58	–4.07	3,190	3,100	21.9	263.4	0.2404	0.711362 (9)	0.70153	0.70189
S18	4.545	35.01	0.0784	0.510334 (9)	–1.95	–3.56	3,180	3,030	11.3	376	0.087	0.706738 (10)	0.70318	0.70331

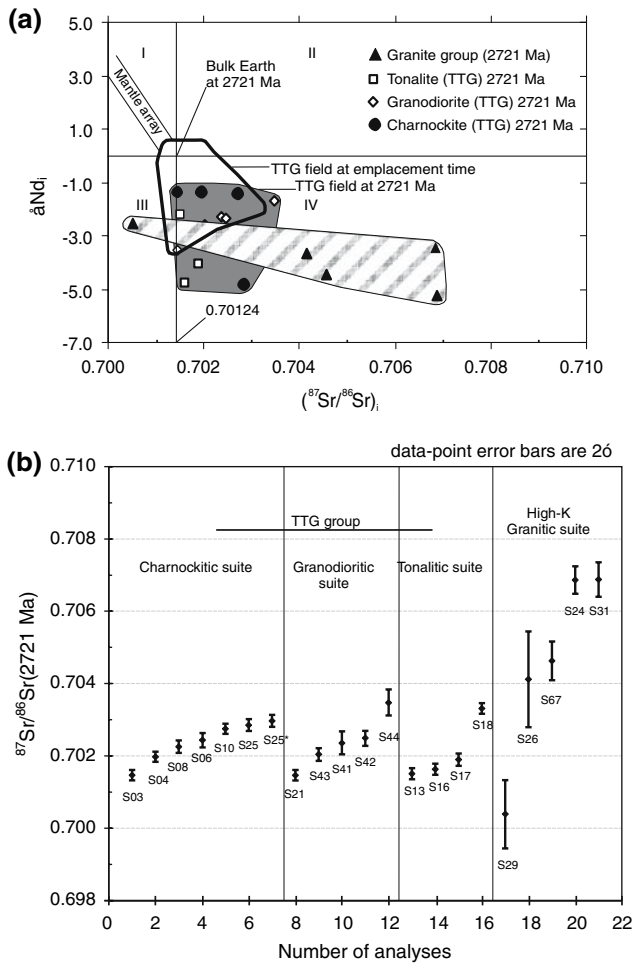

Fig. 12 **a** $\varepsilon Nd_{(T)}$ versus $Sr_{(T)}$ correlation diagram showing the composition of Sangmelima TTG and granitic groups at 2,721 Ma and then the field of TTGs at their emplacement time. Initial Bulk Earth composition of 0.70124 at 2,721 Ma was calculated using present day values from DePaolo (1988) ($^{87}Rb/^{86}Sr = 0.0827$, $^{87}Sr/^{86}Sr = 0.7045$). **b** Diagram of initial $^{87}Sr/^{86}Sr$ at 2,721 Ma, showing dissimilar ratios between granitic suite melts and their TTG source rocks

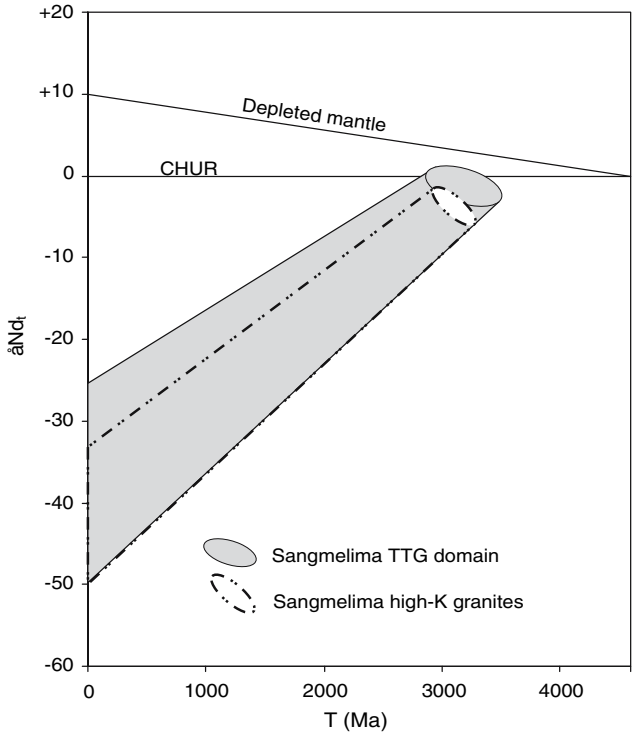

Fig. 13 TDM versus $\varepsilon Nd_{(T)}$ plot showing similar composition and evolution of TTG protolith and their high-K granite melt

melt, a melanosome restite and a palaeosome charnockitic TTG source (Table 4; e.g. Fig. 5a, d) and found a defined relation that gives an indication of element partitioning during partial melting (Table 5). Unsurprisingly, melts are enriched in silica and K_2O compared to restites. Similarly, the melt 89–59C is more enriched in Sr than the restite 89–58A but contrarily to the expected, the restite S36 appears more enriched in Sr than the melt (S35), being consistent with the semi-compatible nature of Sr during low partial melting. This notwithstanding, the restites show enrichment in elements known for their relative immobility while the leucosomic melts are enriched in more mobile elements. However, comparison of element concentration in the melt and restite suggests a low degree of partial melting of the TTG source. But the abundance of high-K granites in the Sangmelima region suggests that despite this low degree of partial melting indice, the necessary condition (e.g. critical melt fraction of about 30–40% required for a felsic melt to separate from its source and define discrete magma bodies, Wickham 1987), was attained during TTG partial melting.

Radiogenic isotope considerations

The high-K granitic group in the Sangmelima region has Sr isotope compositions that are significantly more radiogenic (except for one sample) than Sr isotope compositions of TTG (Fig. 12). This variation in Sr isotopes can mean: (1) that the high-K granite and the TTGs are unrelated, but given field observations (Fig. 5a, d) and the results of major and trace element comparison, there exist little or no doubt that high-K granites are TTG partial melts in the Sangmelima region; (2) that there was sediment/more juvenile material incorporation during granite genesis. Field evidence of metasediment (e.g. Fig. 2a) and amphibolitic xenoliths (e.g. Fig 2b) in Sangmelima TTG suggest that these xenoliths might have contributed to high-K granite magma. (3) That the Sr isotopes were fractionated during melting with ^{87}Sr preferentially going

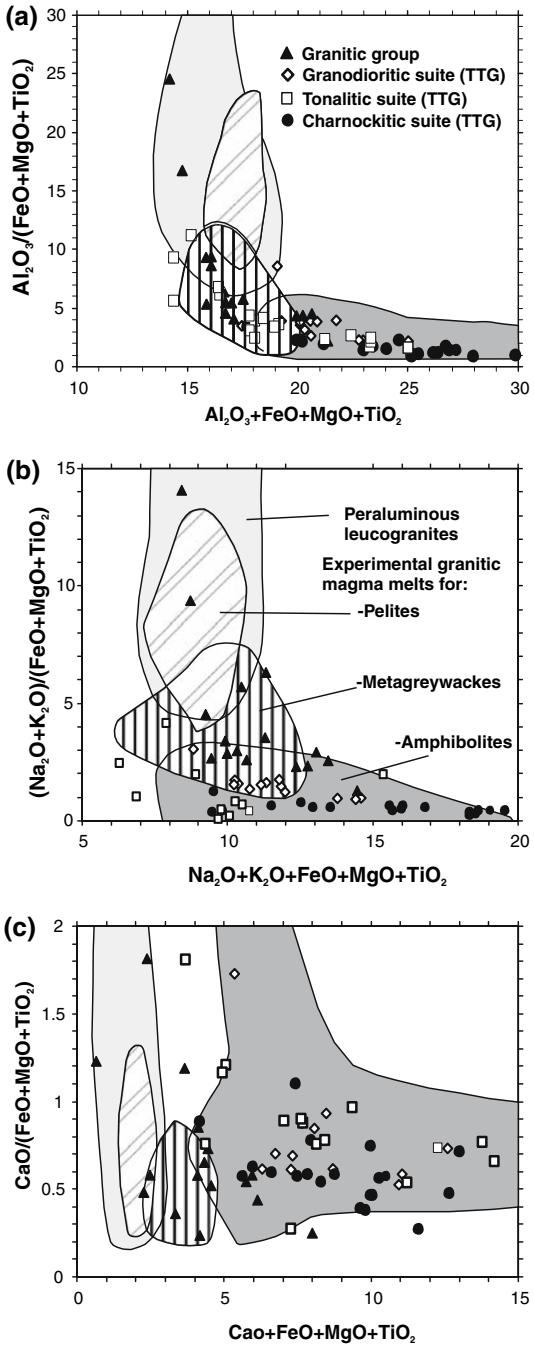

Fig. 14 a–c Geochemical composition of TTG and granitic groups in comparison to compositional fields of experimentally derived partial melts of felsic pelites, metagreywackes and amphibolites (Patiño Douce 1999)

into the melt, cannot be ruled out. In this regard, it is likely that Sr isotope equilibrium was not attained during TTG partial melting.

Following the model of Tommasini and Davies (1997), biotite breakdown would yield melts with high Rb/Sr ratios (K_d Rb and Sr, respectively high and low) and plagioclase derived melts would have relatively low Rb/Sr ratios (K_d Rb and Sr, respectively low and high). Under this model, we would interpret the Sangmelima high-K granites with most radiogenic $^{87}Sr/^{86}Sr$ to represent liquids originating in the melting event dominated by biotite breakdown whereas high-K granites with lower radiogenic $^{87}Sr/^{86}Sr$ could represent liquids with a relatively larger contribution from plagioclase. The observed Sr isotope differences between Sangmelima granitic melts and TTG protolith could therefore imply that despite the extensive mineral reactions and recrystallization associated with the metamorphic event of partial melting, there was no effective equilibration in Sr isotopes between protolith minerals and the melts. Despite this probable disequilibrium in the Sr isotope system, the Nd isotope ratios and $\varepsilon_{Nd,\backslash 2{,}721\ Ma}$ values of some TTG members and the high-K granitic group are similar (Figs. 12, 13). This implies (1) that either the duration of the thermal event was sufficiently long to cause isotopic equilibrium for Nd or (2), that there was no Nd isotopic disequilibrium in the source because all minerals could have had similar parent–daughter Sm/Nd ratios. In addition, Nd model ages are the same for the high-K granitic group and TTGs within error limits, indicating a link between the two rock groups.

It is important to note that the granite low $\varepsilon_{Nd,\backslash 2{,}721\ Ma}$ values (–2.5 to –5.3) suggest that the melting event which produced the high-K granites did not add new mantle material at least to the granitoid budget, as opposed to what the low $Sr_{i,\backslash 2{,}721\ Ma}$ value (0.70036) determined for sample S29 may suggest. This is likely to be rather a local contamination by mafic xenoliths in TTG (e.g. Fig. 2b) than juvenile material input, an indication that the 2,721 Ma high-K granite event was merely a reactivation episode of the existing crust. The younger (2,721 Ma) high-K granites therefore rather inherited their composition from the remobilized-partially melted old (2,825–2,900 Ma) pre-existing TTG crust.

Tectonic setting and heat source

Geochemical data indicate that Sangmelima granitoids belong to (1) the TTG group of a metabasaltic precursor (2) the younger high-K granitic group derived from partially melted TTG. High-K granitoids could indicate major crustal thickening as a result of continental collision (e.g. Treloar et al. 1992) but distinct highly peraluminous character which would be significant in such a setting is absent in Sangmelima high-K granites, despite some Sr isotope and field (Fig. 2a) indices of metasediment contribution. They are predominantly derived from partial melting of igneous TTG sources; the subduction signature represented by

Table 4 Palaeosome-leucosome-restite migmatite association; major elements in wt % and trace elements in ppm

Sample	S32 palaeosome TTG (charnokite)	S35 leucosome melt	S36 restite	89-58B palaeosome TTG (Ch. enderbit)	89-58C leucosome melt	89-58A restite
SiO_2	63.19	81.56	54.06	54.04	74.75	48.17
TiO_2	0.57	0.15	0.99	0.7	0.15	1.4
Al_2O_3	14.28	7.76	14.99	18.04	13.73	13.71
Fe_2O_3	7.75	2.33	13.17	9.32	1.5	15.58
MnO	0.14	0.12	0.21	0.12	0.02	0.22
MgO	4.92	1.99	6.48	3.42	0.55	8.25
CaO	6.02	3.65	7.89	7.89	2.68	7.58
Na_2O	1.48	0.58	0.99	4.91	3.15	2.95
K_2O	0.47	0.25	0.23	0.86	3.24	1.29
P_2O_5	0.05	0.04	0.09	0.32	0.17	0.68
LOI	0.61	0.9	0.46	0.42	0.36	0.62
Total	99.58	99.37	99.69	100	100.3	100.5
$Na_2O + K_2O$	1.95	0.83	1.22	5.77	6.39	4.24
Na_2O/K_2O	3.15	2.32	4.3	5.7	0.97	2.29
A/CNK	1.03	0.99	0.92	0.77	1.01	0.68
Ba	452	229	322	324	2633	366
Cr	138	18	142	46	5	420
Nb	4	7	3	–	–	–
Ni	34	20	66	58	17	171
Rb	43	26	26	8	56	35
Sr	95	24	61	492	444	280
V	157	36	319	193	15	210
Y	15	9	26	15	5	29
Zn	83	24	90	–	–	–
Zr	79	58	77	82	105	136
Sc				33	2	31

Table 5 Comparison of major and trace element partition in melt and restite relative to the source rock (charnockitic TTG, S32 and charnoenderbite 89-58B)

Major elements	SiO_2	TiO_2	Al_2O_3	Fe_2O_3	MnO_2	MgO	CaO	Na_2O	K_2O	P_2O_5
Melt S35	x1.29	x0.26	x0.54	x0.3	x0.86	x0.4	x0.61	x0.4	x0.7	x0.8
Restite S36	x0.85	x1.74	x1.05	x1.7	x1.5	x1.32	x1.31	x0.53	x0.48	x1.8
Melt 89-58C	x1.38	x0.21	x0.76	x0.16	x0.17	x0.16	x0.34	x0.64	x3.77	x0.53
Restite 89-58A	x0.89	x2	x0.76	x1.67	x1.8	x2.44	x0.96	x0.6	x1.5	x2.13
Trace elements	**Ba**	**Cr**	**Nb**	**Ni**	**Rb**	**Sr**	**V**	**Y**	**Zn**	**Zr**
Melt S35	x0.51	x0.13	x1.75	x0.59	x0.61	x0.25	x0.23	x0.6	x0.29	x0.73
Restite S36	x0.71	x1.03	x0.75	x1.94	x0.61	x0.64	x2.03	x1.73	x1.08	x0.98
Melt 89-58C	x8.13	x0.11	–	x0.29	x7	x0.9	x0.08	x0.33	–	x1.28
Restite 89-58A	x1.13	x9.13	–	x2.95	x4.4	x0.6	x1.09	x1.93	–	x1.66

negative Nb and Ti anomalies (Fig. 11a) is therefore an inherited feature from the partially melted TTG source.

We think that mass heat transfer from doleritic magmatism is probably responsible for partial melting-migmatization of TTG and thus responsible for the generation of high-K granites in the Sangmelima region. It is known that basaltic magmas provide heat budget for the partial melting of crustal rocks (e.g. Bullen and Clynne 1990; Roberts and Clemens 1993; Tepper et al. 1993; Guffanti et al. 1996). In fact, doleritic magmatism in the Ntem complex is Archaean (at least the earlier phases; e.g., Fig. 3a; Shang et al. 2006; C.K. Shang et al., in preparation). It is interesting to note that Archaean doleritic magmatism had long been thought to have occurred in the area (e.g. Toteu et al. 1994) even as a younger-Eburnean (2.1 Ga) doleritic generation (e.g., Tchameni 1997; Vicat et al. 1996) has been reported in the eastern part of the Ntem complex, close to the Eburnean Nyong belt (Lerouge et al. 2006). Late Archaean TTG partial melting and the genesis of the high-K granitic group

(2,721 ± 4 Ma; Fig. 3b), would therefore be contemporaneous with the doleritic event (2,723 ± 3.3 Ma; Fig. 3a) and the second deformational tectonics of the Ntem complex that is marked by N0–N45°E sinistral shear planes. High heat flow along these mega shear planes due to linear lithospheric delamination and consequent upwelling of the asthenopshere could be the cause of the doleritic event and in turn of the TTG melting, as proposed for the Hoggar during the Pan-African orogeny (Azzouni-Sekkal et al. 2003; Liégeois et al. 2003). Such a system allows juxtaposing the asthenospheric mantle against the base of the crust, thus allowing to heat the lower crust and does not require Himalayan-type lithospheric thickening. This can occur far from plate boundaries (Azzouni-Sekkal et al. 2003; Liégeois et al. 2003), which is a need in the Sangmelima region where no trace of a subduction event is known at ca. 2.72 Ga, the TTG group being ca. 200 mya older. This is the reason why we do not retain the steepening and the detachment of a subducting slab (e.g. Houseman et al. 1981; Kampunzu et al. 1998) also allowing upwelling of hotter and deeper mantle section, as a valid model in this case.

Conclusions

The Sangmelima granitoids constitute complex calcic to alkalic and magnesian to ferroan composition. The TTGs are marked by both metaluminous and peraluminous composition with their Nd and Sr isotope systematics showing a mantle signature. They were derived from a basaltic protocrust in a subduction setting by partial melting and evolved by fractional crystallization.

High-K granites are the second major granitoid group in the Sangmelima region. They are marked by essentially peraluminous composition. Major element and trace element composition suggests in addition to field observations that they are derived from partial melting of older TTGs. Similar Nd isotopic compositions as well as Nd model ages further support this conclusion despite some discrepancy in Sr isotope composition between the high-K granites and the TTG source rock that is due probably to metavolcanosedimentary input and disequilibrium partial melting of the source rock. Low ε_{Nd} values show that there was no new mantle material input during the genesis of the high-K granitic group in the Congo craton, indicating that this 2,721 Ma event was a reactivation episode of the existing crust. The subduction and related geochemical features of the high-K granites are therefore inherited characteristics from the TTG source rock. The source of heat for partial melting of the older TTG crust at the origin of the high-K granites is contemporaneous mafic doleritic magmatism in the Neoarchaean in the Congo craton caused by the upwelling of the asthenosphere along lithospheric shear zones where linear delamination occurred. Absence of subduction events at the time of the granite generation eliminates the model of the detachment of a steepening subducting slab. In the final analysis, we propose that the evolution of the crust in the Sangmelima region of the Congo craton in late Archaean should be taken to indicate an intracontinental reactivation at 2,721 Ma marked by shear planes probably as a consequence of events occurring at plate boundaries.

Acknowledgments The authors are grateful to Elmar Reitter, G. Bartholomä and M. Schuman, all of the University of Tuebingen for XRF and isotopic analyses and J. Navez of the Central Africa Museum, Tervuren-Belgium, for ICP-MS analyses. Constructive and thorough reviews by B. Ronald Frost, an anonymous reviewer and topic editor Prof. Stern, led to significant improvement of the manuscript. We are very grateful to them. Prof. Dr. Wolf-Christian Dullo and Prof. Stern are highly appreciated for their encouraging statements. CKS would like to express his indebtedness to St. Paulus Catholic Parish, Tuebingen and the Kreim Family, Tuebingen, for hospitality during the course of realization of this study. Much gratitude goes to DAAD for the initial support of this research project.

References

Azzouni-Sekkal A, Liégeois JP, Bechiri-Benmerzoug F, Belaidi-Zinet S, Bonin B (2003) The ''Taourirt'' magmatic province, a marker of the very end of the Pan-African orogeny in the Tuareg Shield: review of the available data and Sr–Nd isotope evidence. J Afr Earth Sci 37:331–350

Barker F (1979) Trondhjemite. Definition, environment and hypotheses of origin. In: Barker F (ed) Trondhjemites, dacites and related rocks. Elsevier, Amsterdam, pp 1–12

Barker F, Arth JG (1976) Generation of trondhjemitic–tonalitic liquids and Achaean bimodal trondhjemites-basalt suites. Geology 4:596–600

Beard JS, Lofgren GE (1991) Dehydration melting and water-saturated melting of basaltic and andesitic greenstones and amphibolites at 1, 3 and 6.9 Kbar. J Petrol 32:365–461

Bessoles B, Trompette R (1980) Géologie de l'Afrique: La Chaîne Pan-Africaine, ''Zone mobile d'Afrique Centrale (partie Sud) et zone Soudanaise''. Mémoire BRGM no. 92

Borg LE, Clynne MA (1998) The petrogenesis of felsic calc-alkaline magmas from the southernmost Cascades, California: origin by partial melting of basaltic lower crust. J Petrol 39:1197–1222

Bullen TD, Clynne MA (1990) Trace element and isotopic constraints on magmatic evolution at Lassen volcanic centre. J Geophys Res 95:19671–19691

Carroll MJ, Wyllie PJ (1989) Experimental phase relations in the system tonalite-peridotite-H_2O at 15 kb; implications for assimilation and differentiation processes near the crust-mantle boundary. J Petrol 30:1351–1382

Chappell BW, White AJR (1984) I and S-type granites in the Lachlan fold belt, southeastern Australia. In: Keqinx GT (eds) Geology of granites and their metalogenetic relations. Scientific Press, Beijing, pp 87–101

Condie KC (1981) Archaean greenstone belts. Elsevier, New York

David K, Schaino P, Allègre CJ (2000) Assessment of the Zr/Hf fractionation in oceanic basalts and continental material during petrogenetic processes. Earth Planet Sci Lett 178:285–301

DePaolo DJ (1988) Neodymium Isotope Geochemistry, An Introduction. In: Minerals and Rocks 20. Springer, Berlin, Heidelberg, New York, pp 1–187

Evans OC, Hanson GN (1992) Most Neoarchaean tonalites, trondhjemites and granodiorites (TTG) in the Superior Province were derived from mantle melts, not melting basalts. Trans Am Geophys Union 73:14–330

Foley S, Tiepolo M, Vannuci R (2002) Growth of early continental crust controlled by melting of amphibolite in subduction zones. Nature 41:837–840

Frost BR, Barnes CG, Collins WJ, Arculus RJ, Ellis DJ, Frost CD (2001) A geochemical classification of granitic rocks. J Petrol 42:2033–2048

Gill JB (1981) Orogenic andesites and plate tectonics. In: PJ Wyllie (ed) Minerals and Rocks vol 16. Springer, Heidelberg, New York, pp 1–390

Glikson AY (1979) Early Precambrian tonalite trondhjemite sialic nuclei. Earth Sci Rev 15:1–73

Goldstein SL, O'Nions RK, Hamilton PJ (1984) A Sm–Nd isotopic study of the atmospheric dust and particulates from major river systems. Earth Planet Sci Lett 70:221–236

Goodwin AM (1991) Precambrian Geology. The dynamic evolution of the continental crust. Academic Press, Harcourt Brace Jovanovich Publishers, New York, pp 1–666

Guffanti M, Clynne MA, Muffler LJP (1996) Thermal and mass implications of magmatic evolution in the Lassen volcanic region, California, and contraints on basalt influx to the lower crust. J Geophys Res 101:3001–3013

Helz R (1976) Phase relations of basalts in their melting ranges at P_{H2O} = 5 kbar: part 2. Melt compositions. J Petrol 17:139–193

Houseman GA, McKenzie DP, Molnar P (1981) Convective instability of a thickened boundary layer and its relevance for the thermal evolution of continental convergent belts. J Geophys Res 86:6115–6132

Jacobson SB, Wasserburg GJ (1980) Sm–Nd isotopic evolution of chondrites. Earth Planet Sci Lett 50:139–155

Jahn BM, Glickson AY, Peucat JJ, Hickman AH (1981) REE geochemistry and isotopic data of Archaean silicic volcanics and granitoids from the Pilbara block, Western Australia: implications for early crustal evolution. Geochim Cosmochim Acta 45:1633–1652

Jahn BM, Auvray B, Shen QH, Liu DY, Zhang ZQ, Dong YJ, Ye XJ, Zhang QZ, Cornichet J, Mace J (1987) Archaean crustal evolution in China: the Taishan complex, and evidence for juvenile crustal addition from long-term depleted mantle. Precam Res 38:381–403

Jayananda M, Martin H, Peucat JJ, Mahabaleswar B (1994) Late Archaean crust–mantle interactions: geochemistry of LREE-enriched mantle derived magmas. Example of the Closepet batholith, Southern India. Contrib Mineral Petrol 119:314–329

Kampunzu AB, Akanyang P, Mapeo RBM, Modie BM, Wendorff M (1998) Geochemistry and tectonic significance of Mesoproterozoic Kgwebe metavolcanic rocks in northwest Botswana: implications for the evolution of the Kibaran Namaqua-Natal belt. Geol Mag 133:669–683

Kampunzu AB, Tombale AR, Zhai M, Bagai Z, Majaule T, Modisi MP (2003) Major and trace element geochemistry of plutonic rocks from Francistown, NE Botswana: evidence for a Neoarchaean continental active margin in the Zimbabwe craton. Lithos 71:431–460

Kay SM, Abbruzzi JM (1996) Magmatic evidence for Neogene lithospheric evolution of the central Andean ''flat-slab'' between 30°S and 32°S. Tectonophysics 259:15–28

Kay SM, Coira B, Viramonte J (1994) Young mafic back arc volcanic rocks as indicators of continental lithospheric delamination beneath the Argentine Puna plateau, Central Andes. J Geophys Res 99(B12):24 323–24 339

Kornprobst J, Lasserre M, Rollet M, Soba D (1976) Existence au Cameroun d'un magmatisme alcalin Pan-Africain ou plus ancien: la syénite néphélinique de Nkonglong. Comparaison avec les roches alcalines connues dans la même région. Bulletin Société Géologique de France, vol 18, no 5, tome XVIII, 1295–1305

Lasserre M, Soba D (1976) Age Libérien des granodiorites et des gneiss à pyroxènes du Cameroun Méridional. Bulletin BRGM 2, no 4, pp 17–32

Le Maitre RW, Bateman P, Dudek A, Keller J, Lameyre MJ, Le Bas PA, Sabine R, Schmid H, Sørenson J, Streckeisen A, Woolley AR, Zanettin B (1989) A classification of igneous rocks and glossary of terms. Blackwell, Oxford, pp 1–193

Lerouge C, Cocherie A, Toteu SF, Penaye J, Milési JP, Tchameni R, Nsifa EN, Fanning M, Deloele E (2006) Shrimp U–Pb zircon age evidence for Paleoproterozoic sedimentation and 2.05Ga syntectonic plutonism in the Nyong Group, South-Western Cameroon: consequences for the Eburnean–Transamazonian belt of NE Brazil and Central Africa. J African Earth Sci 44:413–427

Liégeois JP, Latouche L, Boughrara M, Navez J, Guiraud M (2003) The LATEA metacraton (Central Hoggar, Tuareg shield, Algeria): behaviour of an old passive margin during the Pan-African orogeny. J African Earth Sci 37:161–190

Liew TC, Hofmann AW (1988) Precambrian crustal components, plutonic associations, plate environment of the Hercynian Fold Belt of Central Europe: indications from a Nd and Sr isotopic study. Contrib Mineral Petrol 98:129–138

Lobach-Zhuchenko SB, Chekulaev VG, Arestova NA, Vrevsky AB, Kovalenko AV (2003) Genesis of the earliest (3.20–2.83 Ga) terranes of the Fennoscandian shield. Russian J Earth Sci 5:1–17

Luais B, Hawkesworth CJ (1994) The generation of continental crust; an intergrated study of crust forming processes in the Archaean of Zimbabwe. J Petrol 35:43–93

Lugmair GW, Marti K (1978) Lunar initial $^{143}Nd/^{144}Nd$: differential evolution of the lunar crust and mantle. Earth Planet Sci Lett 39:349–357

Maniar PD, Piccoli PM (1989) Tectonic discrimination of granitoids. Geol Soc Am Bull 101:635–643

Martin H, Chauvel C, Jahn BM (1983) Major and trace element geochemistry and crustal evolution for Archaean granodioritic rocks from Eastern Finland. Precambr Res 21:159–180

Maurizot P, Abessolo A, Feybesse JL, Johan LP (1986) Etude de prospection minière du Sud-Ouest Cameroun. Synthèse des travaux de 1978 à 1985. Rapport de BRGM 85, 274p

Moorbath S, Kamber BS (1998) A reassessment of the timing of early Archaean crustal evolution in West Greenland. Geol Greenland Survey Bull 180:88–93

Mpodozis C, Cornejo P, Kay SM, Titler A (1995) La Franja de Maricunga: Sintesis de la evolucion del Frente Volcanico

Oligoceno-Mioceno de la zona sur de los Andes Centrales. Revista Geol Chile 21:273–313
Nédélec A (1990) Late calc-alkaline plutonism in the Archaean Ntem unit: the Sangmelima granodioritic suite (South Cameroon). 15th colloquium on African Geology, Publications Occasionnelle, CIFEG 22:25–28
Nédélec A, Nsifa EN, Martin H (1990) Major and trace element geochemistry of the Archaean Ntem plutonic complex (South Cameroon): petrogenesis and crustal evolution. Precambr Res 47:35–50
Nsifa EN, Riou R (1990) Post Archaean migmatization in the charnockitic series of the Ntem complex, Congo craton, Southern Cameroon. 15th colloquium on African Geology, Publications Occasionnelle, CIFEG 22:33–36
Nsifa EN, Tchameni R, Belinga SME (1993) De l'existence de formation catarchéennes dans le complexe cratonique du Ntem (Sud-Cameroun), Projet N° 273, Archaean cratonic rocks of Africa. Abstract vol, p 23
O'Connor JT (1965) A classification of quartz rich igneous rocks based on feldspar ratios. US Geol Surv Prof Pap 525B:79–84
Patiño Douce AE (1999) What do experiments tell us about the relative contributions of crust and mantle to the origin of granitic magmas? In Castro A, Fernandez C, Virgneressese JL (Eds). Understanding granites: Intergrating New and Classical techniques. Geol Soc Lond Spec Publ 168:55–75
Patiño Douce AE, Beard JS (1995) Dehydration melting of biotite gneiss and quartz amphibolite from 3 to 15 kbar. J Petrol 36:707–738
Pitcher WS (1993) The nature and origin of granites. Blackie, Glasgow, pp 1–316
Querré G (1985) Palingenèse de la croûte continentale à l'Archéen: les granitoïdes tardifs (2.5–2.4 Ga) de Finlande Orientale. Pétrologie et Géochimie. Mém Doc Centre Arm Et Struct Socles, 2, 226p
Rapp PR (1997) Heterogeneous source regions for Archaean granitoids: experimental and geochemical evidence. In: de Wit MJ, Ashwal LD (eds) Greenstone Belts. Clarendon Press, New York, pp 267–279
Rapp PR, Watson EB, Mille CF (1991) Partial melting of amphobolite/eclogite and the origin of Archaean trondhjemites and tonalites. Precambr Res 94:4619–4633
Roberts MP, Clemens JD (1993) Origin of high-potassium, calc-alkaline, I-type granitoids. Geology 21:825–828
Rocci G (1965) Essai d'interprétation des mesures géochronologiques. La structure de l'Ouest Africain. Science de la Terre France 10:461–479
Roddick JC, Sullivan RW, Dudás FÖ (1992) Precise calibration of Nd tracer isotopic composition for Sm–Nd studies. Chem Geol 97:1–8
Rollinson H (1992) Using geochemical data: evaluation, presentation, interpretation. Longman, London, 352p
Rushmer T (1991) Partial melting of two amphibolites: contrasting experimental results under fluid absent conditions. Contrib Mineral Petrol 107:41–59
Shang CK (2001) Geology, geochemistry and geochronology of Archaean rocks from the Sangmelima Region, Ntem complex, NW Congo Craton, South Cameroon. PhD Thesis, University of Tübingen, Germany, pp1–313
Shang CK, Taubald H, Satir M, Siebel W, Nsifa EN, Vennemann T, Njilah IK, Ghogomu R (2001a) Evidence for a non-cogenetic relationship between monzogranites and TTG suite: Abstract vol EUG XI, Strasbourg, France, p 576
Shang CK, Satir M, Siebel W, Taubald H, Nsifa EN, Westphal M, Reitter E (2001b) Genesis of K-rich granitoids in the Sangmelima region, Ntem Complex (Congo craton), Cameroon. Terra Nostra 5:60–63
Shang CK, Satir M, Siebel W, Nsifa EN, Taubald H, Liégeois JP, Tchoua FM (2004a) Major and trace element geochemistry, Rb–Sr and Sm–Nd systematics of TTG magmatism in the Congo craton: case of the Sangmelima region, Ntem complex, southern Cameroon. J Afr Earth Sci 40:61–79
Shang CK, Siebel W, Satir M, Chen F, Mvondo JO (2004b) Zircon Pb–Pb and U–Pb systematics of TTG rocks in the Congo Craton: constraints of crustal formation, crystallization and Pan-African lead loss. Bull Geosci 79:205–219
Shang CK, Liégeois JP, Satir M, Siebel W, Nsifa EN, Mvondo JO (2006) Zircon Pb loss as a result of a metacratonization process. The case of Sangmelima high-K granitoid zircons, Archaean Ntem complex, Congo craton, southern Cameroon. EGU, Vienna April 2006. Geophys Res Abstracts, vol 8, 03068
Sharma RS, Pankit MK (2003) Evolution of early continental crust. Current Sci 84:995–1001
Shirey S, Hanson GN (1986) Mantle heterogeneity and crustal recycling in Archaean granite-greenstone belts: evidence from Nd isotopes and trace elements in the Rainly Lake area, Superior Province, ON, Canada. Geochem Cosmochim Acta 50:2631–2655
Steiger RH, Jäger E (1977) Subcommision on geochronology: conventions of the use of decay constants in geochronology and cosmochronology. Earth Planet Sci Lett 36:359–362
Stern RN, Hanson GN (1991) Archaean high-Mg granodiorite: a derivative of Light Rare Earth enriched monzodiorite of mantle origin. J Petrol 32:201–238
Sun SS, McDonough WF (1989) Chemical and isotopic systematics of oceanic basalts: implications for mantle composition and processes. In: Saunders AD, Norry MJ (eds). Magmatism in Ocean basins. Geol Soc Lond Spec Publ 42:313–345
Taylor SR, McLennan SM (1985) The continental crust: its composition and evolution. Blackwell, Oxford, pp 312
Tchameni R (1997) Géochimie et géochronologie des formations de l'Archéen et du Paléoprotérozoïque du Sud-Cameroun (Groupe du Ntem, Craton du Congo). Thèse de l'Univérsité d'Orléans, France, pp 1–356
Tchameni R, Mezger K, Nsifa .E, Pouclet A (2000) Neoarchaean evolution in the Congo Craton: evidence from K-rich granitoids of the Ntem Complex, Southern Cameroon. J Afr Earth Sci 30:133–147
Tchameni R, Mezger K, Nsifa NE, Pouclet A (2001) Crustal origin of Early Proterozoic syenites in the Congo craton (Ntem complex), South Cameroon. Lithos 57:23–42
Tepper JH, Nelson BK, Bergantz GW, Irving AJ (1993) Petrology of the Chilliwack batholith, North Cascades, Washington: generation of calc-alkline granitoids by melting of mafic lower crust with variable water fugacity. Contrib Mineral Petrol 113:333–351
Tommasini S, Davies GR (1997) Isotope disequilibrium during anatexis: a case study of contact melting, Siera Nevada, CA. Earth Planet Sci Lett 148:273–285
Toteu SM, Van Schmus WR, Penaye J, Nyobe JB (1994) U–Pb and Sm–Nd evidence for Eburnean and Pan-African high grade metamorphism in cratonic rocks of Southern Cameroon. Precambr Res 67:321–347
Treloar PJ, Coward MP, Harris NBW (1992) Himalayan-Tibetan analogies for the evolution of the Zinbabwe craton and Limpopo belt. Precambr Res 55:571–587
Vicat JP, Leger JM, Nsifa E, Piguet P, Nzenti JP, Tchameni R, Pouclet A (1996) Distinction au sein du craton congolais du Sud-Ouest du Cameroun, de deux épisodes doléritiques initiant les cycles orogéniques éburnéen (Paléoprotérozoïque) et Pan-Africain (Néoprotérozoïque). Compte

Rendu de l'Académie des Sciences, Paris, 323, série IIa:575–582
White AJR, Chappell BW (1977) Ultrametamorphism and granitoid genesis. Tectonophysics 43:7–32
Wickham SM (1987) The generation and emplacement of granitic magmas. J Geol Soc Lond 144:281–297
Wickham SM, Litvinovsky BA, Zanvilevich AN, Bindeman IN (1995) Geochemical evolution of Phanerozoic magmatism in Transbaikalia, East Asia: a key constraint on the origin of K-rich silicic magmas and the process of cratonization. J Geophys Res 100:15641–15654
Windley BF (1998) Tectonic models for the geological evolution of crust, cratons and continents in the Archaean. Revista Brasileira de Geociencias 28(2):183–188
Wolf MB, Wyllie PJ (1994) Dehydration melting of solid amphibolite at 10 kbar: the effect of temperature and time. Contrib Mineral Petrol 115:369–383